Supporting Material

A Human Ventricular Myocyte Model with a Refined Representation of Excitation-Contraction Coupling

Yukiko Himeno,[1] Keiichi Asakura, [1,2] Chae Young Cha,[1, 3] Hiraku Memida,[1] Trevor Powell, [4] Akira Amano, [1] and Akinori Noma [1]

[1]Biosimulation Research Center, College of Life Sciences, Ritsumeikan University,
Noji Higashi 1-1-1 Kusatsu-City, Shiga, Japan
[2]Nippon Shinyaku, Co., Ltd., 14, Nishinosho-Monguchi-cho, Kisshoin, Minami-ku, Kyoto, Japan
[3]Oxford Centre for Diabetes Endocrinology and Metabolism,
University of Oxford, Churchill Hospital, Oxford, OX3 7LJ, UK.
[4]Department of Pharmacology, University of Oxford, Oxford OX1 3QT, UK

The source code of the computer model can be downloaded at http://www.eheartsim.com.

Abbreviations

Table S1. Abbreviations in model equations

V_m	membrane potential (mV)
I_{tot_cell}	total current of ion channels and exchangers (pA/pF)
$I_{tot\_X\_a}$	total current of ion 'X' channels and exchangers at space 'a' (pA/pF)
I_{app_blk}	current applied through a patch electrode (pA/pF)
E_X	reversal potential of ion 'X' , determined by the Nernst equation (mV)
C_m	Whole cell membrane capacitance (pF)

G_I	conductance of current 'I' (pA /pF/mV)
$\mathrm{GHK}_{\mathrm{X\_a}}$	a modified Goldman-Hodgkin-Katz equation of ion 'X' at space 'a' (mM)
k,α,β,ν	rate constants (/ms)
K_{d_X}	dissociation constant for ion 'X' (mM)
$P_{I(\_X)}$	converting factor of current 'I' from $\mathrm{GHK}_{\mathrm{X}}$ (pA/pF /mM)
v_{cyc_T}	turnover rate of transporter 'T' (/ms)
$\mathrm{p(S)}_{(\_\mathrm{a})}$	probability of state 'S' in a scheme of state transitions at space 'a'
V_X	total volume of space 'X' (pL)
$[X_{total}]_a$	total concentration of substance 'X' at space 'a' (mM)
$[X_{free}]_a$	free concentration of substance 'X' at space 'a' (mM)
$[X]_a$	concentration of 'X' at space 'a' (mM)
J_X	total flux of ion 'X' (amol/ms)
z_X	valence of ion 'X'
$\frac{d[X]_a}{dt}$	rate of change of 'X' concentration at space 'a' (mM/ms)

Model parameters

Physical constants

Table S2 Physical constants

R	8.3143	C·mV/mmol/K
T	310	K
F	96.4867	C/mmol

Ion concentrations

Table S3 Ionic composition of external solution

$[K^+]_o$	4.5	mM
$[Na^+]_o$	140	mM
$[Ca^{2+}]_o$	1.8	mM

Substrates (fixed)

Table S4. Substrates

$[MgATP]_{cyt}$	6.631	mM
$[MgADP]_{cyt}$	0.0260	mM
$[Pi]_{cyt}$ (free form)	0.5087	mM
$[H^+]_{cyt}$	0.0001	mM
$[Mg^{2+}]_{cyt}$	0.8	mM
[SPM]	0.005	μM

GHK equation

The magnitudes of ion channel currents are described by the ohmic equation or by the GHK equation. In the latter case, the term to convert mM to pA (permeability times zF) in the original GHK equation is represented by a lumped converting factor, P in a unit of $pA \cdot mM^{-1}$, because of unknown total number of channels within a cell and single channel ion permeability. Then, the fully-activated current amplitude (I) for an ion X is given by,

$$I = P \cdot GHK_X$$

where GHK_X is,

$$GHK_X = \frac{z_X F V_m}{RT} \cdot \frac{\left([X]_i - [X]_o \cdot \exp\left(\frac{-z_X F V_m}{RT} \right) \right)}{\left(1 - \exp\left(\frac{-z_X F V_m}{RT} \right) \right)} .$$

Nernst equation

$$E_X = \frac{R \cdot T}{z_X \cdot F} \cdot \log\left(\frac{[X]_o}{[X]_i} \right)$$

Cell geometry and SR Ca^{2+} compartments

The cell configuration and scalability of the HuVEC model (Sc_Cell)

Almost all models of cardiac myocyte have been developed using a given input capacitance (C_m) and a whole cell volume (V_{cell}). However, the dissociated human ventricular myocytes show a large variety of both cell size (see Fig. 1 in (1)) and the input capacitance (C_m, Fig. S1) as has been obtained in other mammalian species (2). In the present study, we developed a cell model, which can maintain identical characteristics independently of the cell size. Since no human data are available for the relationship between V_{cell} and C_m, we referred to the data (red line in Fig. S1) obtained by Satoh et al., (3), who applied the three-dimensional volume rendering method of confocal images to dissociated rabbit, ferret and rat cells. Though the rat data showed a different slope, we used a slope of 0.197 pL/pF as a first approximation, which is similar to the experimental value of 0.215 pL/pF in both rabbit and ferret. The V_{cell}-C_m relationship (the red line in Fig. S1) was modified to meet the origin. A standard V_{cell} (V_{std} =

37.92 pL) and a C_m (C_{std} = 192.46 pF) were set at a medium size within the range of measurements in human ventricular cells, represented by a rectangular block with a standard size of 120 × 37.62 × 8.4 μm^3, and an input capacitance of 192.46 pF. Note that the range of V_{cell}, calculated over the range of experimental C_m well overlaps with the experimental V_{cell} in Fig. S1. We confirmed that the characteristics of the cell remained unchanged if volume of intracellular Ca^{2+} compartments and rate of Ca^{2+} transfer between SR and the cytosol were scaled by a scaling factor, Sc_Cell = C_m / C_{std}, where C_m is the input capacitance measured in a ventricular cell used in experiments.

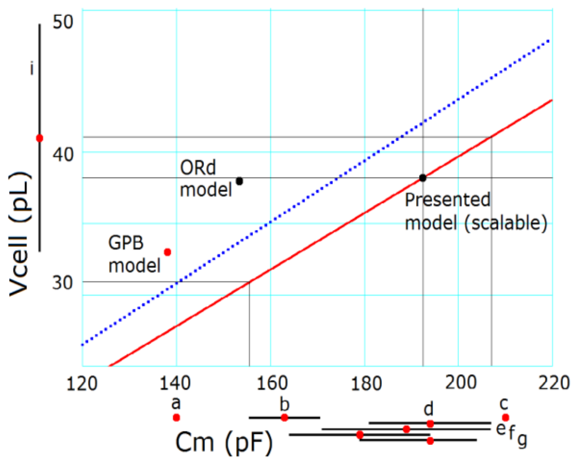

Fig. S1. Relationship between C_m and V_{cell} in the human ventricular cells.

Measurements of the input capacitance C_m of dissociated human ventricular myocyte in various references are indicated along the abscissa by mean values from 2 references (a; (1), c; (4)), or by mean ± SEM from 5 references (b, (1), d; (5), e; (6), f; (7), g; (8)). An experimental measurement of V_{cell} in hearts with normal coronary arteries (9) is indicated with mean ± SEM along the vertical axis. The cell size used in GPB (red point) and ORd (black point) models are indicated in comparison with the thick red line representing the relationship between the V_{cell} and C_m in HuVEC model, given by the following equation. The black point on the red line indicates the standard cell in the present study.

$$V_{cell} = \frac{37.92}{192.46} \cdot C_m$$

The experimental relationship in rabbit ventricular myocytes (3) is shown by the blue dotted line, which is given by,

$$V_{cell} = 0.215 \cdot C_m + 0.718$$

Table S5 compares the volumes of cell as well as Ca^{2+} compartments in HuVEC model with GPB and ORd models. The total volume of SR was set at 6% of V_{cyt} as in ORd model. The volume of SR_{rl} in HuVEC model was adjusted based on two premises [1] $[Ca^{2+}]_{SRrl}$ decreases to less than ~10% of the diastolic level during CICR as assumed in the previous studies (10, 11) in the presence of 3 mM calsequestrin (2.6 and 10 mM in GPB and ORd model, respectively), and [2] CICR results in a peak amplitude of ~0.5 μM for the global Ca^{2+} transients in the presence of Ca^{2+} uptake by SERCA and myoplasmic Ca^{2+} buffers including troponin, calmodulin, ATP as well as fixed binding sites on the T-tubule and SR membranes as in GPB model.

Table S5 Cell geometry compared with previous models

	GPB model	ORd model	HuVEC model
Cell configuration (cell volume)	(V_{cell}) Cylinder L = 100 μm, r = 10.25 μm (= 33 pL)	(V_{cell}) Cylinder L = 100 μm, r = 11 μm (= 38 pL)	(V_{cell}) Scalable rectangular block L = 120 μm, W = 37.62 μm, D = 8.4 μm (= 37.92 pL)
Bulk space	(V_{myo}) 65% V_{cell} (= 21.45 pL)	(v_{myo}) 68% V_{cell} (= 25.84 pL)	(V_{blk}) 68% V_{cell} (= 25.79 pL)
Total SR space	(V_{sr}) 3.5% V_{cell} (= 1.16 pL)	(V_{sr}) 6% V_{cell} (= 2.28 pL)	(V_{sr}) 6% V_{cell} (= 2.28 pL)
SR releasing site volume	-	(V_{jsr}) 0.48 % V_{cell} (= 0.182 pL)	(V_{SRrl}) 1.2 % V_{cell} (= 0.46 pL)
SR uptake site volume	-	(V_{nsr}) 5.52 % V_{cell} (= 2.098 pL)	(V_{SRup}) 4.8 % V_{cell} (= 1.82 pL)
Junction space	(V_{junc}) 0.0539 % V_{cell} (= 0.0178 pL)	-	(V_{jnc} + V_{nd}) 0.8 % V_{cell} (= 0.30 pL)
Subsarcolemmal space	(V_{sl}) 2% V_{cell} (= 0.66 pL)	(V_{ss}) 2 % V_{cell} (= 0.76 pL)	(V_{iz}) 3.5 % V_{cell} (= 1.33 pL)
Diffusion conductivity	$G_{Caslmyo}$ = 3724 fL/ms	G_{dca_ssmyo} = 3800 fL/ms	G_{dCa_jnciz} = 3396 fL/ms and G_{dCa_izblk} = 3508 fL/ms
Input capacitance	138.1 pF	153.4 pF	192.46 pF

Ca^{2+} buffer

The detailed set of buffer species (12) used in the GPB model was adopted after several simplifications as described in our previous paper (13). In short, we deleted the myosin, Na^+ and Mg^{2+} buffers, and fixed $[Mg^{2+}]$. The low affinity binding of Ca^{2+} to troponin (TnCl) was replaced by a contraction model (14) and the amount of the high affinity site (TnCh) was adjusted.

Bulk space (*blk*)

$$\frac{d[CaMCa]}{dt} = k_{on\_CaM} \cdot [Ca^{2+}]_{blk} \cdot ([B_{total}CaM] - [CaMCa]) - k_{off\_CaM} \cdot [CaMCa]$$

$k_{off\_CaM} = 0.238$, $k_{on\_CaM} = 34$

$$\frac{d[TnChCa]}{dt} = k_{on\_TnCh} \cdot [Ca^{2+}]_{blk} \cdot ([B_{total}TnCh] - [TnChCa]) - k_{off\_TnCh} \cdot [TnChCa]$$

$k_{off\_TnCh} = 0.000032$, $k_{on\_TnCh} = 2.37$

$$\frac{d[SRCa]}{dt} = k_{on\_SR} \cdot [Ca^{2+}]_{blk} \cdot ([B_{total}SR] - [SRCa]) - k_{off\_SR} \cdot [SRCa]$$

$k_{off\_SR} = 0.06$, $k_{on\_SR} = 100$

Intermediate zone (*iz*)

$$[L_{free}]_{iz} = \frac{[B_{total}L]_{iz}}{1+\frac{[Ca^{2+}]_{iz}}{K_{dL\_iz}}}$$

$$K_{dL\_jiz} = \frac{k_{off\_L\_iz}}{k_{on\_L\_iz}}, k_{off\_L\_iz} = 1.3,\ k_{on\_L\_iz} = 100$$

$$[H_{free}]_{iz} = \frac{[B_{total}H]_{iz}}{1+\frac{[Ca^{2+}]_{iz}}{K_{dH\_iz}}}$$

$$K_{dH\_iz} = \frac{k_{off\_H\_iz}}{k_{on\_H\_iz}},\ k_{off\_H\_iz} = 0.03,\ k_{on\_H\_iz} = 100$$

$$[Ca^{2+}]_{iz} = \frac{[Ca_{tot}]_{iz}}{1+\frac{[Lf]_{iz}}{K_{dL\_iz}}+\frac{[Hf]_{iz}}{K_{dH\_iz}}}$$

Junctional space (*jnc*)

$$[L_{free}]_{jnc} = \frac{[B_{total}L]_{jnc}}{1+\frac{[Ca^{2+}]_{jnc}}{K_{dL\_jnc}}}$$

$$K_{dL\_jnc} = \frac{k_{off\_L\_jnc}}{k_{on\_L\_jnc}},\ k_{off\_L\_jnc} = 1.3,\ k_{on\_L\_jnc} = 100$$

$$[H_{free}]_{jnc} = \frac{[B_{total}H]_{jnc}}{1+\frac{[Ca^{2+}]_{jnc}}{K_{dH\_jnc}}}$$

$$K_{dH\_jnc} = \frac{k_{off\_H\_jnc}}{k_{on\_H\_jnc}},\ k_{off\_H\_jnc} = 0.03,\ k_{on\_H\_jnc} = 100$$

$$[Ca^{2+}]_{jnc} = \frac{[Ca_{tot}]_{jnc}}{1+\frac{[Lf]_{jnc}}{K_{dL\_jnc}}+\frac{[Hf]_{jnc}}{K_{dH\_jnc}}}$$

Release site of the SR (*SRrl*)

$$K_{d\_CSQN\_Ca} = \frac{k_{off\_CSQN}}{k_{on\_CSQN}}$$

$$k_{off\_CSQN} = 65,\ \ k_{on\_CSQN} = 100$$

$$a = 1$$

$$b = [B_{total}CSQN] - [Ca^{2+}_{total}]_{SRrl} + K_{d\_CSQN\_Ca}$$

$$c = -K_{d\_CSQN\_Ca} \cdot [Ca^{2+}_{total}]_{SRrl}$$

$$[Ca^{2+}]_{SRrl} = \frac{-b+\sqrt{b^2-4\cdot a\cdot c}}{2\cdot a}$$

Boundary Ca^{2+} diffusion

Ca^{2+} transfer between cytosolic compartments

$$J_{Ca\_jnciz} = G_{dCa\_jnciz} \cdot ([Ca^{2+}]_{jnc} - [Ca^{2+}]_{iz}) \cdot \text{Sc\_Cell}$$

$$G_{dCa\_jnciz} = 3395.88 \ \ (fL \cdot ms^{-1})$$

$$J_{Ca\_izblk} = G_{dCa\_izblk} \cdot ([Ca^{2+}]_{iz} - [Ca^{2+}]_{blk}) \cdot \text{Sc\_Cell}$$

$$G_{dCa\_jzblk} = 3507.78 \ \ (fL \cdot ms^{-1})$$

Ca^{2+} transfer from SR uptake site to release site

$$J_{trans\_SR} = P_{trans} \cdot ([Ca^{2+}]_{SRup} - [Ca^{2+}]_{SRrl}) \cdot Sc\_cell$$

$$P_{trans} = 4.8037$$

Ion channels and transporters

L-type Ca^{2+} current (I_{CaL}, LCC)

We used the scheme of Shirokov *et al*. (1993) and Ferreira *et al*. (1997), in which Ca^{2+}, passing through the channel itself, takes the primary role in the Ca^{2+}-mediated inactivation (15-18). The same 4-state model was used for both LCCs in CaRU (I_{CaL_jnc}) and for LCCs located in *iz* (I_{CaL_iz}) and *blk* (I_{CaL_blk}). The $[Ca^{2+}]_{nd}$ determined by Eqs. 2 or S150-S153 were used to calculate the Ca^{2+}-mediated inactivation for I_{CaL_jnc}, and $[Ca^{2+}]_{nd}$ determined by Eqs. S175, S176 for I_{CaL_iz} and I_{CaL_blk}. This $[Ca^{2+}]_{nd}$ is ~10 times-higher than the average $[Ca^{2+}]_{jnc}$ in HuVEC or $[Ca^{2+}]$ in the Ca^{2+} compartments ($[Ca^{2+}]_{jnc}$ in GPB or $[Ca^{2+}]_{ss}$ in GPB models) obtained by the time-integration of fluxes in the cleft space in most of cardiac cell models. The rate constants for the V_m-gate (α_+ and α_-) and Ca^{2+}-gate (ε_+ and ε_-) of LCC are given by Eqs. S1, S2 and Eqs. S5, S6, respectively. Both of the activation (α_+) and deactivation (α_-) rates of the V_m-gate were described as a function of two exponential terms, and adjusted to human data (see activation curve (chocolate) superimposed on experimental data in Fig. S2A, B).

$$\alpha_+ = \frac{1}{3.734 \cdot Exp(-\frac{V_m}{8.5}) + 0.35 \cdot Exp(-\frac{V_m}{3500})} \qquad \text{(Eq. S1)}$$

$$\alpha_- = \frac{1}{4.65 \cdot Exp(\frac{V_m}{15}) + 1.363 \cdot Exp(\frac{V_m}{100})} \qquad \text{(Eq. S2)}$$

The rate constant (ε_+) for the Ca^{2+}-inactivation was determined according to the Hinch algorithm. The inactivation rate ε_+ could be divided into two terms by integrating Eq. S3 with S4.

$$\tilde{\alpha}_+ = \frac{\exp(\frac{V_m - V_L}{\Delta V_L})}{t_L \cdot (\exp(\frac{V_m - V_L}{\Delta V_L}) + 1)} \qquad \text{(Eq. S3)}$$

$$\tilde{\varepsilon}_+ = \frac{[Ca^{2+}]_{nd} \cdot (\exp(\frac{V_m - V_L}{\Delta V_L}) + a)}{\tau_L \cdot \tilde{K}_L (\exp(\frac{V_m - V_L}{\Delta V_L}) + 1)} = \frac{[Ca^{2+}]_{nd} \cdot t_L \cdot \tilde{\alpha}_+}{\tau_L \cdot \tilde{K}_L} + \frac{[Ca^{2+}]_{nd} \cdot a}{\tau_L \cdot \tilde{K}_L (\exp(\frac{V_m - V_L}{\Delta V_L}) + 1)} \quad \text{(Eq. S4)}$$

where V_L is defined as a potential when half LCC open, ΔV_L width of opening potentials, t_L time switching between C and O states, τ_L, inactivation time, K_L concentration at inactivation and a biasing to make inactivation function of V. To avoid confusion, α, ε and K_L from Hinch model were given a tilde. The first term of Eq. S4 is a function of both $[Ca^{2+}]_{nd}$, the activation rate of V_m-gate ($\tilde{\alpha}_+$) and V_m. The second term is a sigmoidal function of V_m, increasing with increasing negativity of V_m toward a saturation level, unlikely in experiments. Therefore, the second term was removed for simplicity, and Eq. S5 was used in our model.

$$\varepsilon_+ = \frac{[Ca^{2+}]_{nd} \cdot \alpha_+}{T_L \cdot K_L} \quad , \quad \text{(Eq. S5)}$$

where α_+ is given by Eq. S1 and τ_L/t_L in Eq. S4 was substituted by T_L.

$T_L = 147.51$

In the revised model, the values of T_L (= 147.51) and K_L (=0.0044 mM) (or the product of $T_L \times K_L$) for ε_+, and a new equation for ε_- (Eq. S5 and S6) were determined by referring to the experimental measurements of steady-state inactivation (Fig. S2_B) and time constants (Fig. S2_C3) described in literatures (see legends of Fig. S2 for references). The value of $[Ca^{2+}]_{nd}$ (Ca_{L0}, or Ca_{LR}) shown in Fig. S2C1 was determined by Eq. S152 or S153, respectively, at a representative $[Ca^{2+}]_{SRrl}$ of 0.7 mM and a $[Ca^{2+}]_{jnc}$ of 0.0001 mM. The ε_+ was calculated at four different values of $[Ca]_{SRrl}$ (0.71, 0.51, 0.31, 0.11 mM) as shown in Fig. S2_B and S2_C, since $[Ca]_{SRrl}$ might be different in experimental conditions and thereby caused variations in the data of I_{CaL} inactivation. The rate of removing Ca^{2+} inactivation (ε_-) was determined by referring to the recovery rate from the inactivation at the resting potential in Fig. S2C3 and the V_m-dependence of steady-state inactivation in B.

$$\varepsilon\_ = \frac{1}{8084 \cdot Exp(\frac{V_m}{10}) + 158 \cdot Exp(\frac{V_m}{1000})} + \frac{1}{134736 \cdot Exp(-\frac{V_m}{5}) + 337 \cdot Exp(-\frac{V_m}{2000})} \quad \text{(Eq. S6)}$$

The $[Ca^{2+}]_{nd}$ for LCC located in *iz* and *blk* were calculated in the same way as in CaRU.

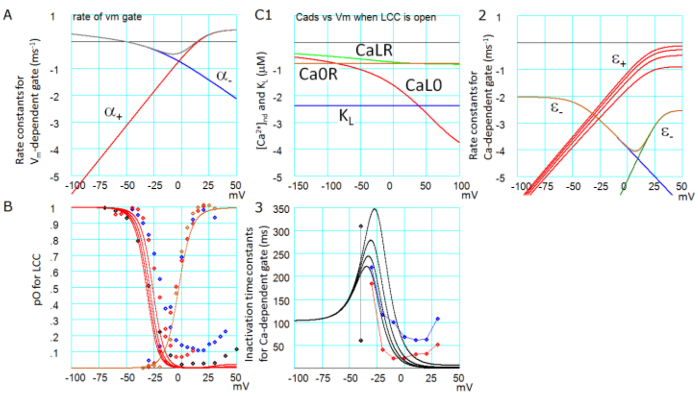

Fig. S2. Determination of LCC gating from the experimental data

A: activation (α_+, red) and deactivation rate constants (α_-, blue) and the sum of the two rate constants (1 / τ, gray). B: the steady-state activation and inactivation of LCC. Data points are from Mewes & Ravens (6) (red), Pelzmann et al. (19) (blue), Magyar et al. (20) (chocolate) and Li et al., (21) (black). C1: the $[Ca^{2+}]_{nd}$ –V_m relations were calculated for Ca_{L0} (red), Ca_{LR} (gray), and Ca_{0R} (chocolate) together with K_L in Eq. S5 (blue). C2: the inactivation rate (at Ca_{L0}) plotted for four $[Ca]_{SRrl}$ (ε_+, red curves), and removal rate from inactivation (ε_-, chocolate curves) given by the two components in Eq. S6. C3: the V_m-dependence of Ca^{2+}-inactivation τ. Data points are from Beukelmann et al.(1) (red), Pelzmann (19) (blue), Fulop et al., (22) (a single chocolate point) and Pelzmann (19) (black points connected with gray line are the fast and slow components).

$$pO_{LCC\_a} = Y_{ooo} + Y_{ooc} \qquad \text{(Eq. S7)}$$

$$I_{CaL\_X\_a} = f_{CaL\_a} \cdot P_{CaL\_X} \cdot GHK_{X\_a} \cdot pO_{LCC\_a} \cdot \frac{1}{1+(\frac{1.4}{[ATP]})^3} \qquad \text{(Eq. S8)}$$

a = (blk, iz, jnc), X = (Ca, Na, K). [ATP] was fixed to 6 mM.

Fraction of I_{CaL}

$f_{CaL\_jnc} = 0.75$, $f_{CaL\_blk} = 0.10$, $f_{CaL\_iz} = 0.15$

Converting factors

$P_{CaL\_Ca} = 14.21$

$P_{CaL\_Na} = 0.0000185 \cdot P_{CaL\_Ca}$

$P_{CaL\_K} = 0.000367 \cdot P_{CaL\_Ca}$

$$I_{CaL} = (I_{CaL\_Ca\_jnc} + I_{CaL\_Na\_jnc} + I_{CaL\_K\_jnc}) + (I_{CaL\_Ca\_iz} + I_{CaL\_Na\_iz} + I_{CaL\_K\_iz}) + (I_{CaL\_Ca\_blk} + I_{CaL\_Na\_blk} + I_{CaL\_K\_blk}) \qquad \text{(Eq. S9)}$$

Ca^{2+}-mediated inactivation in other models for comparison

Ca^{2+}-mediated inactivation in ORd model was examined under the widely used assumption that the I_{Ba} through LCC was solely due to VDI. This assumption is different from the thorough experimental conclusion by Brunet *et al.* (23) and Ferreira *et al.* (18) (see also Discussion in Grandi *et al.* (24)). Ferreira *et al*, (18) recorded I_{Ba} in the transfected cell-line with the pore-forming α1 subunit in association with β subunits, and revealed that the I_{Ba} decayed as the sum of two exponentials, where the first one (τ = 600 ms at 21 ºC) was accompanied with no gating current, but the slow one (τ = 6 s) was with the gating current, indicating that the former is CDI and the latter is VDI. Brunet *et al.* (23) suggested that the CDI of I_{Ba} is mediated by a low affinity binding of Ba^{2+} to calmodulin as has been suggested in foregoing studies (18, 25, 26), and indicated that unambiguous measurement of VDI requires use of Na^+ or another monovalent cation as charge carrier (for the slow inactivation of I_{Na} via LCC, see Matsuda (27)). In HuVEC model, we simply ignored the relatively slow inactivation of I_{Na} for the sake of simplicity.

The time course of LCC inactivation during AP was conventionally examined by recording compensation currents (I_{cp}) during the I_{CaL} blockage in the AP clamp experiment. However, our simulation of the AP clamp indicated (not shown) that I_{cp} is not equal to I_{CaL}, but represents a sum of modifications of all current components, such as I_{CaL}, I_{NCX}, I_{Ks}, I_{Cab}, $I_{L(ca)}$ and I_{PMCA} caused by blocking the Ca^{2+}-flux of I_{CaL}.

Sodium current (I_{Na})

The same I_{Na} model as in our previous study (13) was used, except for the amplitude parameters, f_L and P_{Na}. I_{Na} is composed of the two components, I_{NaT} and I_{NaL}.

$$I_{Na} = I_{NaT} + I_{NaL} \tag{Eq. S10}$$

Transient component (I_{NaT})

$$\frac{dp(C)_{NaT}}{dt} = k_{OC} \cdot p(O)_{NaT} + k_{I2C} \cdot p(I_2)_{NaT} + k_{Isb} \cdot p(I_s)_{NaT} - (k_{Isf} - f_{C\_Na} \cdot (k_{C2O} + k_{C2I2})) \cdot p(C)_{NaT} \tag{Eq. S11}$$

$$\frac{\mathrm{dp(O)_{NaT}}}{\mathrm{dt}} = \mathrm{k_{I2O}} \cdot \mathrm{p(I_2)_{NaT}} + \mathrm{f_{C\_Na}} \cdot \mathrm{k_{C2O}} \cdot \mathrm{p(C)_{NaT}} - (\mathrm{k_{OC}} + \mathrm{k_{OI2}}) \cdot \mathrm{p(O)_{NaT}} \tag{Eq. S12}$$

$$\frac{\mathrm{dp(I_2)_{NaT}}}{\mathrm{dt}} = \mathrm{f_{C\_Na}} \cdot \mathrm{k_{C2I2}} \cdot \mathrm{p(C)_{NaT}} + \mathrm{k_{OI2}} \cdot \mathrm{p(O)_{NaT}} + \mathrm{k_{Isb}} \cdot \mathrm{p(I_s)_{NaT}} - (\mathrm{k_{I2C}} + \mathrm{k_{I2O}} + \mathrm{k_{Isf}}) \cdot \mathrm{p(I_2)_{NaT}} \tag{Eq. S13}$$

$$\frac{\mathrm{dp(I_s)_{NaT}}}{\mathrm{dt}} = \mathrm{k_{Isf}} \cdot \mathrm{p(I_2)_{NaT}} + \mathrm{k_{Isf}} \cdot \mathrm{p(C)_{NaT}} - 2 \cdot \mathrm{k_{Isb}} \cdot \mathrm{p(I_s)_{NaT}} \tag{Eq. S14}$$

$$f_{C\_Na} = \frac{C_2}{(C_1 + C_2)} = \frac{1}{1 + \exp\left(-\frac{V_m + 48}{7}\right)} \tag{Eq. S15}$$

$$k_{C2O} = \frac{1}{0.0025 \cdot \exp\left(\frac{V_m}{-8.0}\right) + 0.15 \cdot \exp\left(\frac{V_m}{-100.0}\right)} \tag{Eq. S16}$$

$$k_{OC} = \frac{1}{30.0 \cdot \exp\left(\frac{V_m}{12.0}\right) + 0.53 \cdot \exp\left(\frac{V_m}{50.0}\right)} \tag{Eq. S17}$$

$$k_{OI2} = \frac{1}{0.0433 \cdot \exp\left(\frac{V_m}{-27.0}\right) + 0.34 \cdot \exp\left(\frac{V_m}{-2000.0}\right)} \tag{Eq. S18}$$

$$k_{I2O} = 0.0001312$$

$$k_{C2I2} = \frac{0.5}{1.0 + \frac{k_{I2O} \cdot k_{OC}}{k_{OI2} \cdot k_{C2O}}} \tag{Eq. S19}$$

$$k_{I2C} = 0.5 - k_{C2I2} \tag{Eq. S20}$$

$$k_{Isb} = \frac{1}{300000.0 \cdot \exp\left(\frac{V_m}{10.0}\right) + 50000.0 \cdot \exp\left(\frac{V_m}{16.0}\right)} \tag{Eq. S21}$$

$$k_{Isf} = \frac{1}{0.016 \cdot \exp\left(\frac{V_m}{-9.9}\right) + 8.0 \cdot \exp\left(\frac{V_m}{-45.0}\right)} \tag{Eq. S22}$$

$$\mathrm{I_{NaT}} = (1 - \mathrm{f_L}) \cdot \mathrm{P_{Na}} \cdot (\mathrm{GHK_{Na}} + 0.1 \cdot \mathrm{GHK_K}) \cdot \mathrm{p(O)_{NaT}} \tag{Eq. S23}$$

Late component (I_{NaL})

The k_{I1I2}, k_{OI1}, k_{I1O}, k_{I1C} and k_{C2I1} are specific for I_{NaL}, and other rate constants are the same as in I_{NaL}.

$$\frac{dp(C)_{NaL}}{dt} = k_{OC} \cdot p(O)_{NaL} + k_{I1C} \cdot p(I_1)_{NaL} + k_{I2C} \cdot p(I_2)_{NaL} + k_{Isb} \cdot p(I_s)_{NaL} - \left(k_{Isf} + f_{C\_Na} \cdot \left(k_{C2O} + k_{C2I2} + k_{C2I1}\right)\right) \cdot p(C)_{NaL} \quad \text{(Eq. S24)}$$

$$\frac{dp(O)_{NaL}}{dt} = k_{I1O} \cdot p(I_1)_{NaL} + f_{C\_Na} \cdot k_{C2O} \cdot p(C)_{NaL} - \left(k_{OC} + k_{OI1}\right) \cdot p(O)_{NaL} \quad \text{(Eq. S25)}$$

$$\frac{dp(I_1)_{NaL}}{dt} = k_{OI1} \cdot p(O)_{NaL} + f_{C\_Na} \cdot k_{C2I1} \cdot p(C)_{NaL} - \left(k_{I1O} + k_{I1C} + k_{I1I2}\right) \cdot p(I_1)_{NaL} \quad \text{(Eq. S26)}$$

$$\frac{dp(I_2)_{NaL}}{dt} = f_{C\_Na} \cdot k_{C2I2} \cdot p(C)_{NaL} + k_{I1I2} \cdot p(I_1)_{NaL} + k_{Isb} \cdot p(I_s)_{NaL} - \left(k_{I2C} + k_{Isf}\right) \cdot p(I_2)_{NaL} \quad \text{(Eq. S27)}$$

$$\frac{dp(I_s)_{NaL}}{dt} = k_{Isf} \cdot p(I_2)_{NaL} + k_{Isf} \cdot p(C)_{NaL} - 2 \cdot k_{Isb} \cdot p(I_s)_{NaL} \quad \text{(Eq. S28)}$$

$k_{I1I2} = 0.00534$

$k_{OI1} = k_{OI2}$

$k_{I1O} = 0.01$

$k_{I1C} = k_{I2C}$

$k_{C2I1} = k_{C2I2}$

$$I_{NaL} = f_L \cdot P_{Na} \cdot \left(GHK_{Na} + 0.1 \cdot GHK_K\right) \cdot p(O)_{NaL} \quad \text{(Eq. S29)}$$

$f_L = 0.13125$, $P_{Na} = 8.1072$ (pA/mM)

Inward rectifier potassium current (I_{K1})

The characteristic inward-going rectification of I_{K1} has been widely observed in mammalian ventricular cells, including human cells. Yan and Ishihara (28) and Ishihara and Yan (29) conducted detailed analysis using transfected 293T cell line and demonstrated the time-dependent kinetic changes in I_{K1} (I_{K1} transient) on repolarization to -30~-50 mV, and explained it by the time lag between the instantaneous relief of Mg^{2+}-block and the relatively slow spermine-block during AP repolarization. We adopted this model after adjusting the amplitude of I_{K1} to obtain a maximum repolarizing rate of ~1 V/s. $[Mg^{2+}]_{cyt}$ fixed at 0.8 mM for the Mg^{2+}-block in the mode 1, and spermine concentration [SPM] = 5 μM.

$$\alpha_{Mg} = 12.0 \cdot \exp\left(-0.025 \cdot \left(V_m - E_K\right)\right) \quad \text{(Eq. S30)}$$

$$\beta_{Mg} = 28 \cdot [Mg^{2+}]_{cyt} \cdot \exp\left(0.025 \cdot \left(V_m - E_K\right)\right) \quad \text{(Eq. S31)}$$

$$f_O = \frac{\alpha_{Mg}}{\alpha_{Mg} + \beta_{Mg}} \quad \text{(Eq. S32)}$$

$$f_B = \frac{\beta_{Mg}}{\alpha_{Mg} + \beta_{Mg}} \quad \text{(Eq. S33)}$$

$$po_{Mg} = f_O \cdot f_O \cdot f_O \quad \text{(Eq. S34)}$$

$$po_{Mg1} = 3.0 \cdot f_O \cdot f_O \cdot f_B \quad \text{(Eq. S35)}$$

$$po_{Mg2} = 3.0 \cdot f_O \cdot f_B \cdot f_B \quad \text{(Eq. S36)}$$

The SPM-block in the mode 2

$$\alpha_{SPM} = \frac{0.17\cdot\exp\left(-0.07\cdot\left((V_m-E_K)+8\cdot[Mg^{2+}]_{cyt}\right)\right)}{1.0+0.01\cdot\exp\left(0.12\cdot\left((V_m-E_K)+8\cdot[Mg^{2+}]_{cyt}\right)\right)} \qquad \text{(Eq. S37)}$$

$$\beta_{SPM} = \frac{0.28\cdot[SPM]\cdot\exp\left(0.15\cdot\left((V_m-E_K)+8\cdot[Mg^{2+}]_{cyt}\right)\right)}{1.0+0.01\cdot\exp\left(0.13\left((V_m-E_K)+8\cdot[Mg^{2+}]_{cyt}\right)\right)} \qquad \text{(Eq. S38)}$$

$$\frac{\mathrm{dPb_{spm}}}{\mathrm{dt}} = \beta_{SPM}\cdot po_{Mg}\cdot(1-Pb_{spm})-\alpha_{SPM}\cdot Pb_{spm} \qquad \text{(Eq. S39)}$$

$$po_{mode\,1} = f_{mode\,1}\cdot(1-Pb_{spm})\cdot\left(po_{Mg}+\frac{2}{3}\cdot po_{Mg1}+\frac{1}{3}\cdot po_{Mg2}\right) \qquad \text{(Eq. S40)}$$

$$f_{mode\,1} = 0.9$$

$$po_{mode\,2} = \frac{(1-f_{mode\,1})}{1.0+\frac{[SPM]}{40.0\cdot exp\left(-\frac{Vm-E_K}{9.1}\right)}} \qquad \text{(Eq. S41)}$$

$$p(O)_{K1} = po_{mode\,1}+po_{mode\,2} \qquad \text{(Eq. S42)}$$

$$\chi_{K1} = \frac{\left(\frac{[K^+]_o}{4.5}\right)^{0.4}}{1.0+\exp\left(-\frac{[K^+]_o-2.2}{0.6}\right)} \qquad \text{(Eq. S43)}$$

$$I_{K1} = G_{K1}\cdot\chi_{K1}\cdot(V_m-E_K)\cdot p(O)_{K1} \qquad \text{(Eq. S44)}$$

$$G_{K1} = 1.353$$

Delayed rectifier K$^+$ current, fast component (I_{Kr})

Different models of I_{Kr} were used in the GPB and ORd models. We adopted the ORd I_{Kr} model, which was developed by referring to the slow inactivation kinetics of I_{Kr} demonstrated in Iost *et al.* (8) and Jost *et al.* (4). We adjusted the amplitude of I_{Kr} to a medium size of I_{Kr} tail currents at -40 or -30 mV among different references (0.25 in Iost et al. (8); 0.29 in Jost *et al.* (30), 0.57 in Jost *et al.* (4), 0.31 in Magyar *et al.* (20), 0.32 in Li *et al.* (7), and 0.25 pA/pF in Rajamani *et al.* (31)). The experimental prolongation of APD_{90} was well reconstructed by blocking I_{Kr} (with a limiting amplitude of ~0.3 pA/pF), which is less than a half of that in ORd model of 0.85 pA/pF (see Results, Fig. 3A1 red and 4 blue).

$$X_{r,\infty} = \frac{1}{1+exp\left(\frac{-(Vm+8.337)}{6.789}\right)} \qquad \text{(Eq. S45)}$$

$$\tau_{Xr,fast} = 12.98+\frac{1}{0.3652\cdot exp\left(\frac{Vm-31.66}{3.869}\right)+4.123\cdot10^{-5}\cdot exp\left(\frac{-(Vm-47.78)}{20.38}\right)} \qquad \text{(Eq. S46)}$$

$$\tau_{Xr,slow} = 1.865+\frac{1}{0.06629\cdot exp\left(\frac{Vm-34.70}{7.355}\right)+1.128\cdot10^{-5}\cdot exp\left(\frac{-(Vm-29.74)}{25.94}\right)} \qquad \text{(Eq. S47)}$$

$$A_{Xr,fast} = \frac{1}{1+exp\left(\frac{Vm+4.81}{38.21}\right)} \qquad \text{(Eq. S48)}$$

$$A_{Xr,slow} = 1-A_{Xr,fast} \qquad \text{(Eq. S49)}$$

$$\frac{dX_{r,fast}}{dt} = \frac{X_{r,\infty}-X_{r,fast}}{\tau_{Xr,fast}} \qquad \text{(Eq. S50)}$$

$$\frac{dX_{r,slow}}{dt} = \frac{X_{r,\infty}-X_{r,slow}}{\tau_{Xr,slow}} \qquad \text{(Eq. S51)}$$

$$X_r = A_{Xr,fast}\cdot X_{r,fast}+A_{Xr,slow}\cdot X_{r,slow} \qquad \text{(Eq. S52)}$$

$$R_{Kr} = \frac{1}{\left(1+exp\left(\frac{V_m+55}{75}\right)\right)\cdot\left(1+exp\left(\frac{V_m-10}{30}\right)\right)} \quad \text{(Eq. S53)}$$

$$p(O)_{Kr} = X_r \cdot R_{Kr} \quad \text{(Eq. S54)}$$

$$\chi_{Kr} = \sqrt{\frac{[K^+]_o}{4.5}} \quad \text{(Eq. S55)}$$

$$I_{Kr} = G_{Kr} \cdot \chi_{Kr} \cdot (V_m - E_K) \cdot p(O)_{Kr} \quad \text{(Eq. S56)}$$

$$G_{Kr} = 0.0166$$

Delayed rectifier K+ current, slow component (I_{Ks})

The gating kinetics of ORd model was used after separating I_{Ks} into two components, I_{Ks_K} and I_{Ks_Na} and using the GHK equation. The permeability ratio, $P_{Na} : P_K = 0.04 : 1$.

$$para_{Xs1\_a,\infty} = \frac{1}{1+exp\left(\frac{-(V_m+11.60)}{8.932}\right)} \quad \text{(Eq. S57)}$$

$$\tau_{Xs1\_a} = 817.3 + \frac{1}{2.326\cdot10^{-4}\cdot exp\left(\frac{V_m+48.28}{17.80}\right)+0.001292\cdot exp\left(\frac{-(V_m+210.0)}{230.0}\right)} \quad \text{(Eq. S58)}$$

$$\frac{dpara_{Xs1\_a}}{dt} = \frac{para_{Xs1\_a,\infty}-para_{Xs1\_a}}{\tau_{Xs1\_a}} \quad \text{(Eq. S59)}$$

$$para_{Xs2\_a,\infty} = para_{Xs1\_a,\infty} \quad \text{(Eq. S60)}$$

$$\tau_{Xs2\_a} = \frac{1}{0.01\cdot exp\left(\frac{V_m-50}{20}\right)+0.0193\cdot exp\left(\frac{-(V_m+66.54)}{31}\right)} \quad \text{(Eq. S61)}$$

$$\frac{dpara_{Xs2\_a}}{dt} = \frac{para_{Xs2\_a,\infty}-para_{Xs2\_a}}{\tau_{Xs2\_a}} \quad \text{(Eq. S62)}$$

$$para_{RKs\_a} = 1 + \frac{0.6}{1+\left(\frac{0.000038}{[Ca^{2+}]_a}\right)^{1.4}} \quad \text{(Eq. S63)}$$

$$p(O)_{Ks\_a} = para_{xs1\_a} \cdot para_{xs2\_a} \cdot para_{RKs\_a} \quad \text{(Eq. S64)}$$

$$I_{Ks\_X\_a} = f_{Ks\_a} \cdot P_{Ks\_X} \cdot GHK_X \cdot p(O)_{Ks\_a} \quad \text{(Eq. S65)}$$

a = (blk, iz), X = (K, Na)

$f_{Ks\_iz} = 0.1$, $f_{Ks\_blk} = 0.9$

Converting factors

$P_{Ks\_K} = 0.002782$, $P_{Ks\_Na} = 0.04 \cdot P_{Ks\_K}$

$$I_{Ks} = (I_{Ks\_K\_iz} + I_{Ks\_Na\_iz}) + (I_{Ks\_K\_blk} + I_{Ks\_Na\_blk}) \quad \text{(Eq. S66)}$$

Transient outward K+ current (I_{Kto})

The gating kinetics of the ORd model was used after adjusting G_{Kto}.

$$a_\infty = \frac{1}{1+exp\left(\frac{-(V_m-14.34)}{14.82}\right)} \quad \text{(Eq. S67)}$$

$$\tau_a = \frac{1.0515}{\frac{1}{1.2089\cdot\left(1+exp\left(\frac{-(V_m-18.41)}{29.38}\right)\right)}+\frac{3.5}{1+exp\left(\frac{V_m+100}{29.38}\right)}} \quad \text{(Eq. S68)}$$

$$\frac{da}{dt} = \frac{a_\infty - a}{\tau_a} \quad \text{(Eq. S69)}$$

$$i_\infty = \frac{1}{1+exp\left(\frac{V_m+43.94)}{5.711}\right)} \quad \text{(Eq. S70)}$$

$$\tau_{i,fast} = 4.562 + \frac{1}{0.3933\cdot exp\left(\frac{-(V_m+100)}{100}\right)+0.08004\cdot exp\left(\frac{V_m+50)}{16.59}\right)} \quad \text{(Eq. S71)}$$

$$\tau_{i,slow} = 23.62 + \frac{1}{0.001416\cdot exp\left(\frac{-(V_m+96.52)}{59.05}\right)+1.7808\cdot 10^{-8}\cdot exp\left(\frac{V_m+114.1}{8.079}\right)} \quad \text{(Eq. S72)}$$

$$A_{i,fast} = \frac{1}{1+exp\left(\frac{V_m-213.6}{151.2}\right)} \quad \text{(Eq. S73)}$$

$$A_{i,slow} = 1 - A_{i,fast} \quad \text{(Eq. S74)}$$

$$\frac{di_{fast}}{dt} = \frac{i_\infty - i_{fast}}{\tau_{i,fast}} \quad \text{(Eq. S75)}$$

$$\frac{di_{slow}}{dt} = \frac{i_\infty - i_{slow}}{\tau_{i,slow}} \quad \text{(Eq. S76)}$$

$$i = A_{i,fast}\cdot i_{fast} + A_{i,slow}\cdot i_{slow} \quad \text{(Eq. S77)}$$

$$p(O)_{Kto} = a\cdot i \quad \text{(Eq. S78)}$$

$$I_{Kto} = G_{Kto}\cdot p(O)_{Kto}\cdot\left(V_m - E_K\right) \quad \text{(Eq. S79)}$$

$$G_{Kto} = 0.0312$$

Time-independent currents

All these currents are from Takeuchi *et al.* (32) as described in Asakura *et al.* (13).

Voltage-dependent potassium current (plateau current) (I_{Kpl})

$$p(O)_{Kpl} = \frac{V_m}{1-exp\left(-\frac{V_m}{13.0}\right)} \quad \text{(Eq. S80)}$$

$$\chi_{Kpl} = \left(\frac{[K^+]_o}{5.4}\right)^{0.16} \quad \text{(Eq. S81)}$$

$$I_{Kpl} = P_{Kpl}\cdot\chi_{Kpl}\cdot p(O)_{Kpl}\cdot GHK_K \quad \text{(Eq. S82)}$$

$$P_{Kpl} = 0.0000172$$

Background calcium current (I_{Cab})

$$I_{Cab\_a} = P_{Cab\_a}\cdot f_{Cab\_a}\cdot GHK_{Ca}\ ,\quad a = (blk,\ iz) \quad \text{(Eq. S83)}$$

$$P_{Cab\_a} = 0.00006822$$

Fraction of I_{Cab}

$f_{Cab\_iz} = 0.1$, $f_{Cab\_blk} = 0.9$

$$I_{Cab} = I_{Cab\_iz} + I_{Cab\_blk}$$
(Eq. S84)

Background non-selective cation current (I_{bNSC})

$$I_{bNSC\_X} = P_{bNSC\_X} \cdot GHK_X \;, \quad X = (K,\ Na)$$
(Eq. S85)

$P_{bNSC\_K} = 0.00014$, $P_{bNSC\_Na} = 0.00035$

$$I_{bNSC} = I_{bNSC\_K} + I_{bNSC\_Na}$$
(Eq. S86)

Calcium-activated background cation current ($I_{l(Ca)}$)

$$\mathrm{p(O)_a} = \frac{1.0}{1.0 + \left(\frac{0.0012}{[\mathrm{Ca}^{2+}]_\mathrm{a}}\right)^3}$$
(Eq. S87)

$$I_{l(Ca)\_X\_a} = P_{l(Ca)\_X} \cdot f_{l(Ca)\_a} \cdot GHK_X \cdot p(O)_a \qquad X = (Na,\ K), \quad a = (blk,\ iz)$$
(Eq. S88)

$P_{l(Ca)\_Na} = 0.00273$

$P_{l(Ca)\_K} = P_{l(Ca)\_Na}$

Fraction of $I_{l(Ca)}$

$f_{l(Ca)\_iz} = 0.1$, $f_{l(Ca)\_blk} = 0.9$

$$I_{l(Ca)} = I_{l(Ca)\_Na\_iz} + I_{l(Ca)\_K\_iz} + I_{l(Ca)\_Na\_blk} + I_{l(Ca)\_K\_blk}$$
(Eq. S89)

ATP-sensitive potassium current (I_{KATP})

$$\mathrm{p(O)_{KATP}} = \frac{0.8}{1.0 + \left(\frac{[\mathrm{ATP}]_\mathrm{cyt}}{0.1}\right)^2}$$
(Eq. S90)

$$\chi_{KATP} = 0.0236 \cdot \left([K^+]_o\right)^{0.24}$$
(Eq. S91)

$$I_{KATP} = G_{KATP} \cdot (V_m - E_K) \cdot p(O)_{KATP} \cdot \chi_{KATP}$$
(Eq. S92)

$G_{KATP} = 17.674$

Na^+/K^+ pump current (I_{NaK})

As described in PBMB, the Na^+/K^+ pump model developed by Oka *et al.* (33) on the framework of Smith and Crampin (34) was used after adjusting Amp_{NaK}.

$$\overline{\mathrm{Na}_i} = \frac{[\mathrm{Na}^+]_i}{K_{d,Nai}}$$
(Eq. S93)

$$\overline{\mathrm{Na}_o} = \frac{[\mathrm{Na}^+]_o}{K_{d,Nao}}$$
(Eq. S94)

$$\overline{\mathrm{K}_i} = \frac{[\mathrm{K}^+]_i}{K_{d,Ki}}$$
(Eq. S95)

$$\overline{\mathrm{K}_o} = \frac{[\mathrm{K}^+]_o}{K_{d,Ko}}$$
(Eq. S96)

$$\overline{\mathrm{MgATP}} = \frac{[MgATP]_{cyt}}{K_{d,MgATP}}$$ (Eq. S97)

$$K_{d,Nao} = K^0_{d,Nao} \cdot \exp\frac{\Delta_{Nao} \cdot FV_m}{RT}$$ (Eq. S98)

$$K_{d,Nai} = K^0_{d,Nai} \cdot \exp\frac{\Delta_{Nai} \cdot FV_m}{RT}$$ (Eq. S99)

$$K_{d,Ko} = K^0_{d,Ko} \cdot \exp\frac{\Delta_{Ko} \cdot FV_m}{RT}$$ (Eq. S100)

$$K_{d,Ki} = K^0_{d,Ki} \cdot \exp\frac{\Delta_{Ki} \cdot FV_m}{RT}$$ (Eq. S101)

$K^0_{d,Nai} = 5$, $K^0_{d,Nae} = 26.8$, $K^0_{d,Ki} = 18.8$, $K^0_{d,Ke} = 0.8$, $K_{d,MgATP} = 0.6$

$\Delta_{Nai} = -0.14$, $\Delta_{Nao} = 0.44$, $\Delta_{Ki} = -0.14$, $\Delta_{Ko} = 0.23$

$$\alpha_1^+ = \frac{k_1^+ \overline{\mathrm{Na}_i}^3}{(1+\overline{\mathrm{Na}_i})^3 + (1+\overline{\mathrm{K}_i})^2 - 1}$$ (Eq. S102)

$$\alpha_2^+ = k_2^+$$ (Eq. S103)

$$\alpha_3^+ = \frac{k_3^+ \overline{\mathrm{K}_o}^2}{(1+\overline{\mathrm{Na}_o})^3 + (1+\overline{\mathrm{K}_o})^2 - 1}$$ (Eq. S104)

$$\alpha_4^+ = \frac{k_4^+ \overline{\mathrm{MgATP}}}{1+\overline{\mathrm{MgATP}}}$$ (Eq. S105)

$$\alpha_1^- = k_1^- [MgADP]_{cyt}$$ (Eq. S106)

$$\alpha_2^- = \frac{k_2^- \overline{\mathrm{Na}_o}^3}{(1+\overline{\mathrm{Na}_o})^3 + (1+\overline{\mathrm{K}_o})^2 - 1}$$ (Eq. S107)

$$\alpha_3^- = \frac{k_3^- [\mathrm{Pi}][\mathrm{H}^+]}{1+\overline{\mathrm{MgATP}}}$$ (Eq. S108)

$$\alpha_4^- = \frac{k_4^- \overline{\mathrm{K}_i}^2}{(1+\overline{\mathrm{Na}_i})^3 + (1+\overline{\mathrm{K}_i})^2 - 1}$$ (Eq. S109)

$k_1^+ = 0.72$, $k_1^- = 0.08$, $k_2^+ = 0.08$, $k_2^- = 0.008$, $k_3^+ = 4$, $k_3^- = 8000$, $k_4^+ = 0.3$, $k_4^- = 0.2$ (Eq. S110)

$$\frac{dP_7}{dt} = -\alpha_2^+ \cdot P_7 + \alpha_2^- \cdot P_{8\_13} + \alpha_1^+ \cdot P_{1\_6} - \alpha_1^- \cdot P_7$$ (Eq. S111)

$$\frac{dP_{8\_13}}{dt} = -\alpha_3^+ \cdot P_{8\_13} + \alpha_3^- \cdot P_{14\_15} + \alpha_2^+ \cdot P_7 - \alpha_2^- \cdot P_{8\_13}$$ (Eq. S112)

$$V_{step1} = \alpha_1^+ \cdot P_{1\_6} - \alpha_1^- \cdot P_7$$ (Eq. S113)

$$V_{step2} = \alpha_2^+ \cdot P_7 - \alpha_2^- \cdot P_{8\_13}$$ (Eq. S114)

$$V_{step3} = \alpha_3^+ \cdot P_{8\_13} - \alpha_3^- \cdot P_{14\_15}$$ (Eq. S115)

$$V_{step4} = \alpha_4^+ \cdot P_{14\_15} - \alpha_4^- \cdot P_{1\_6}$$
(Eq. S116)

$$v_{cyc\_NaK} = V_{step2}$$
(Eq. S117)

$$I_{NaK} = Amp_{NaK} \cdot v_{cyc\_NaK}$$
(Eq. S118)

$$Amp_{NaK} = 25.178$$

$$I_{NaK\_Na} = Stoi_{NaK\_Na} \cdot I_{NaK} \qquad Stoi_{NaK\_Na} = 3, \quad I_{NaK\_K} = Stoi_{NaK\_K} \cdot I_{NaK}$$
(Eq. S119)

$$Stoi_{NaK\_K} = -2$$
(Eq. S120)

Na^+/Ca^{2+} exchange current (I_{NCX})

The NCX model developed by Takeuchi *et al.* (32) was used after adjusting the amplitude factor Amp_{NCX}.

a = (blk, iz)

$$\alpha_{1\_a} = q_a(E_1Na) \cdot \left(f_{Caina\_a} \cdot \alpha_{1\_on} + (1 - f_{Caina\_a}) \cdot \alpha_{1\_off} \right)$$
(Eq. S121)

$$\beta_{1\_a} = f_{Caina\_a} \cdot \beta_{1\_on} + (1 - f_{Caina\_a}) \cdot \beta_{1\_off}$$
(Eq. S122)

$$\alpha_{2\_a} = f_{Caina\_a} \cdot \alpha_{2\_on} + (1 - f_{Caina\_a}) \cdot \alpha_{2\_off}$$
(Eq. S123)

$$\beta_{2\_a} = f_{Caina\_a} \cdot \beta_{2\_on} + (1 - f_{Caina\_a}) \cdot \beta_{2\_off}$$
(Eq. S124)

$$\alpha_{1\_on} = 0.002, \quad \alpha_{1\_off} = 0.0015, \quad \beta_{1\_on} = 0.0012, \quad \beta_{1\_off} = 0.0000005$$

$$\alpha_{2\_on} = 0.00006, \quad \alpha_{2\_off} = 0.02, \quad \beta_{2\_on} = 0.18 \quad \beta_{2\_off} = 0.0002$$

$$\alpha_E = k_2 \cdot q(E_2Na) + k_4 \cdot q(E_2Ca)$$
(Eq. S125)

$$\beta_{E\_a} = k_1 \cdot q_a(E_1Na) + k_3 \cdot q_a(E_1Ca)$$
(Eq. S126)

$$\mathrm{k_1} = \exp\left(\frac{0.32 \cdot \mathrm{F} \cdot \mathrm{V_m}}{\mathrm{R} \cdot \mathrm{T}}\right)$$
(Eq. S127)

$$\mathrm{k_2} = \exp\left(\frac{(0.32 - 1) \cdot \mathrm{F} \cdot \mathrm{V_m}}{\mathrm{R} \cdot \mathrm{T}}\right)$$
(Eq. S128)

$$k_3 = 1.0, \quad k_4 = 1.0$$

$$f_{Caina\_a} = \frac{[Ca^{2+}]_a}{[Ca^{2+}]_a + K_{m,act}}$$
(Eq. S129)

$$K_{m,act} = 0.004$$

$$\frac{dp(E_1)_{NCX\_a}}{dt} = p(E_2)_{NCX\_a} \cdot \alpha_E + p(I_1)_{NCX\_a} \cdot \beta_{1\_a} + p(I_2)_{NCX\_a} \cdot \beta_{2\_a} - p(E_1)_{NCX\_a} \cdot (\beta_{E\_a} + \alpha_{1\_X} + \alpha_{2\_X})$$

(Eq. S130)

$$\frac{dp(I_1)_{NCX\_a}}{dt} = p(E_1)_{NCX\_a} \cdot \alpha_{1\_a} - p(I_1)_{NCX\_a} \cdot \beta_{1\_a}$$

(Eq. S131)

$$\frac{dp(I_2)_{NCX\_a}}{dt} = p(E_1)_{NCX\_a} \cdot \alpha_{2\_a} - p(I_2)_{NCX\_a} \cdot \beta_{2\_a}$$

(Eq. S132)

$$p(E_2)_{NCX\_a} = 1 - p(E_1)_{NCX\_a} - p(I_1)_{NCX\_a} - p(I_2)_{NCX\_a}$$

(Eq. S133)

$$q_a(E_1Na) = \frac{1.0}{\left(1.0 + \left(\frac{K_{m.Nai}}{[Na^+]_i}\right)^3\right) \cdot \left(1.0 + \frac{[Ca^{2+}]_a}{K_{m,Cai}}\right)}$$

(Eq. S134)

$$q_a(E_1Ca) = \frac{1.0}{\left(1.0 + \frac{K_{m,Cai}}{[Ca^{2+}]_a}\right) \cdot \left(1.0 + \left(\frac{[Na^+]_i}{K_{m,Nai}}\right)^3\right)}$$

(Eq. S135)

$$q(E_2Na) = \frac{1.0}{\left(1.0 + \left(\frac{K_{m,Nao}}{[Na^+]_o}\right)^3\right) \cdot \left(1.0 + \frac{[Ca^{2+}]_o}{K_{m,Cao}}\right)}$$

(Eq. S136)

$$q(E_2Ca) = \frac{1.0}{\left(1.0 + \frac{K_{m,Cao}}{[Ca^{2+}]_o}\right) \cdot \left(1.0 + \left(\frac{[Na^+]_o}{K_{m,Nao}}\right)^3\right)}$$

(Eq. S137)

$K_{m,Nao} = 87.5$, $K_{m,Nai} = 20.74854$, $K_{m,Cao} = 1.38$, $K_{m,Cai} = 0.0184$

$$v_{cyc\_NCX\_a} = k_1 \cdot q_a(E_1Na) \cdot p(E_1)_{NCX\_a} - k_2 \cdot q_a(E_2Na) \cdot p(E_2)_{NCX\_a}$$

(Eq. S138)

$$I_{NCX\_a} = f_{NCX\_a} \cdot Amp_{NCX} \cdot v_{cyc\_NCX\_a}$$

(Eq. S139)

$Amp_{NCX} = 30.53$

$$I_{NCX} = I_{NCX\_iz} + I_{NCX\_blk}$$

(Eq. S140)

$f_{NCX\_iz} = 0.1$, $f_{NCX\_blk} = 0.9$

$$I_{NCX\_Na\_a} = 3 \cdot I_{NCX\_a}$$

(Eq. S141)

$$I_{NCX\_Ca\_a} = -2 \cdot I_{NCX\_a}$$

(Eq. S142)

Plasma membrane Ca^{2+}-ATPase current (I_{PMCA})

The model equation used in Grandi *et al*. (35) was used for spaces *iz* and *blk* after adjusting the amplitude factor Amp_{PMCA} and K_m.

$$I_{PMCA\_a} = f_{PMCA\_a} \cdot Amp_{PMCA} \cdot \frac{\left([Ca^{2+}]_a\right)^{1.6}}{\left(K_m\right)^{1.6} + \left([Ca^{2+}]_a\right)^{1.6}} \qquad \text{(Eq. S143)}$$

a = (blk, iz)

$f_{PMCA\_iz} = 0.1$, $f_{PMCA\_blk} = 0.9$, $Amp_{PMCA} = 0.19$, Km=0.0005

$$I_{PMCA} = I_{PMCA\_iz} + I_{PMCA\_blk} \qquad \text{(Eq. S144)}$$

CaRU

LCC

The tightly coupled LCC-RyR kinetic model developed by Hinch *et al.* (36) was used after modifications. The new LCC model is described in the section L-type Ca^{2+} current.

RyR channel

The state transition of a RyR is defined by the two–state transition with the activation rate, k_{co} and deactivation rate k_{oc}.

$$kco = Q_{10} \cdot \frac{0.4}{1 + (\frac{0.025}{[Ca^{2+}]_{nd}})^{2.7}} \qquad \text{(Eq. S145)}$$

The $[Ca^{2+}]_{nd}$ for the activation is,
$[Ca^{2+}]_{nd} = Ca_{L0}$ for LCC-dependent activation of a RyR
$[Ca^{2+}]_{nd} = Ca_{00}$ for spontaneous activation of a RyR

$$koc = Q_{10} \cdot 0.5664 \qquad \text{(Eq. S146)}$$

$$f_t = \frac{k_{co}}{k_{co} + k_{oc}} \qquad \text{(Eq. S147)}$$

The state transition of couplon at the regenerative step is also described by the two-state transition scheme.

$$Closed \underset{k_{roc}}{\overset{k_{rco}}{\rightleftarrows}} Open$$

The activation rate k_{rco} and the deactivation rate k_{roc} are,

$$k_{rco} = f_n \cdot f_t \cdot k_{co} \cdot (sloc0 + [Ca^{2+}]_{SRrl}) \qquad \text{(Eq. S148)}$$

$f_n = 7$, $sloc0 = 0.1$
$[Ca^{2+}]_{nd} = Ca_{LR}$ for LCC-dependent activation,
$[Ca^{2+}]_{nd} = Ca_{0R}$ for RyR-dependent spontaneous activation,

$$k_{roc} = k_{oc} \cdot pC^{((N_{RyR}-1)\cdot 0.74)} \qquad pC = \frac{k_{oc}}{k_{oc} + f_t \cdot \dfrac{k_{rco}}{f_n}} \tag{Eq. S149}$$

The f_t in Eq. S149 is calculated using Ca_{00}. N_{RyR} is the number of RyRs in a couplon and assumed to be 10.

The $[Ca^{2+}]_{nd}$ (indicated in Fig. 1) is defined as Ca_{00}, Ca_{0R}, Ca_{L0} or Ca_{LR}.
LCC closed; RyR closed:

$$Ca_{00} = [Ca^{2+}]_{jnc} \tag{Eq. S150}$$

LCC closed; RyR open:

$$Ca_{0R} = \frac{Ca_{00} + f_R \cdot [Ca^{2+}]_{SRrl}}{1 + f_R} \tag{Eq. S151}$$

$$f_R = 0.31$$

LCC open; RyR closed:

$$Ca_{L0} = \frac{Ca_{00} + f_L \cdot \dfrac{\delta V \cdot e^{-\delta V}}{1 - e^{-\delta V}} \cdot [Ca^{2+}]_o}{(1 + f_L \cdot \dfrac{\delta V}{1 - e^{-\delta V}})} \tag{Eq. S152}$$

$$f_L = 0.014$$

LCC open; RyR open:

$$Ca_{LR} = \frac{Ca_{00} + f_R \cdot [Ca^{2+}]_{SRrl} + f_L \cdot \dfrac{\delta V \cdot e^{-\delta V}}{1 - e^{-\delta V}} \cdot [Ca^{2+}]_o}{1 + f_R + f_L \cdot \dfrac{\delta V}{1 - e^{-\delta V}}} \tag{Eq. S153}$$

$$\delta = \frac{2 \cdot F}{R \cdot T} \tag{Eq. S154}$$

$$p(O)_t = p(O) + p(O)_{base} \tag{Eq. S155}$$

$$p(O)_{base} = 0.000075$$

$$p(O) = Y_{ooo} + Y_{coo} + Y_{cco} + Y_{oco} \tag{Eq. S156}$$

$$J_{Ca\_rel} = P_{RyR} \cdot p(O)_t \cdot ([Ca^{2+}]_{SRrl} - [Ca^{2+}]_{jnc}) \cdot Sc\_cell \tag{Eq. S157}$$

$$P_{RyR} = 5967.67 \ \ (fL \cdot ms^{-1}) \qquad \text{(whole cell)}$$

Sarcoplasmic reticulum Ca^{2+} pump (SERCA) current (J_{SERCA})

The three-state model developed by Tran *et al.* (37) was used after several minor modifications as described in Asakura *et al.* (2014) (13). The limiting amplitude of J_{SERCA}, ampSERCA, was modified.

$$\alpha 1 = 25900 \cdot [\mathrm{MgATP}] \quad \text{(Eq. S158)}$$

$$\alpha 2 = \frac{2540}{1 + \left(\frac{Kd_{Cai}}{[Ca^{2+}]_{blk}}\right)^{1.7}} \quad \text{(Eq. S159)}$$

K_{dCai} = 0.0027 (mM)

$$\alpha 3 = \frac{5.35}{1 + \left(\frac{[Ca^{2+}]_{SRup}}{Kd_{Casr}}\right)^{1.7}} \quad \text{(Eq. S160)}$$

K_{dCasr} = 1.378 (mM)

$$\beta 1 = \frac{0.1972}{1 + \left(\frac{[Ca^{2+}]_{blk}}{Kd_{Cai}}\right)^{1.7}} \quad \text{(Eq. S161)}$$

$$\beta 2 = \frac{25435 \cdot [MgADP]_{cyt}}{1 + \left(\frac{Kd_{Casr}}{[Ca^{2+}]_{SRup}}\right)^{1.7}} \quad \text{(Eq. S162)}$$

$$\beta 3 = 149 \cdot [\mathrm{Pi}] \quad \text{(Eq. S163)}$$

$$v_{cyc} = \frac{6.86 \cdot (\alpha 1 \cdot \alpha 2 \cdot \alpha 3 - \beta 1 \cdot \beta 2 \cdot \beta 3)}{\alpha 2 \cdot \alpha 3 + \beta 1 \cdot \alpha 3 + \beta 1 \cdot \beta 2 + \alpha 1 \cdot \alpha 3 + \beta 2 \cdot \alpha 1 + \beta 2 \cdot \beta 3 + \alpha 1 \cdot \alpha 2 + \beta 3 \cdot \beta 1 + \beta 3 \cdot \alpha 2} \quad \text{(Eq. S164)}$$

$$J_{SERCA} = \frac{ampSERCA \cdot v_{cyc}}{2 \cdot F} \cdot Sc\_cell \quad \text{(Eq. S165)}$$

ampSERCA = 106.4448 (mmol.ms^{-1})

Rate of change in the membrane potential and ion concentrations

Membrane potential

$$\frac{dV_m}{dt} = -\left(I_{tot\_cell} + I_{app}\right) \quad \text{(Eq. S166)}$$

$$I_{tot\_cell} = I_{tot\_Na} + I_{tot\_Ca} + I_{tot\_K} \quad \text{(Eq. S167)}$$

$$I_{tot\_Ca} = I_{tot\_Ca\_jnc} + I_{tot\_Ca\_iz} + I_{tot\_Ca\_blk} \quad \text{(Eq. S168)}$$

$$I_{tot\_Ca\_jnc} = I_{CaL\_Ca\_LR} + I_{CaL\_Ca\_L0} \quad \text{(Eq. S169)}$$

$$I_{tot\_Ca\_iz} = I_{CaL\_Ca\_iz} + I_{PMCA\_iz} + I_{NCX\_Ca\_iz} + I_{Cab\_iz} \quad \text{(Eq. S170)}$$

$$I_{tot\_Ca\_blk} = I_{CaL\_Ca\_blk} + I_{PMCA\_blk} + I_{NCX\_Ca\_blk} + I_{Cab\_blk} \quad \text{(Eq. S171)}$$

$$I_{tot\_Na} = \left(I_{CaL\_Na\_jnc} + I_{CaL\_Na\_iz} + I_{CaL\_Na\_blk}\right) + \left(I_{NCX\_Na\_iz} + I_{NCX\_Na\_blk}\right) + \left(I_{Ks\_Na\_iz} + I_{Ks\_Na\_blk}\right) + I_{NaT\_Na} + I_{NaL\_Na} + I_{NaK\_Na} + I_{Kto\_Na} + I_{bNSC\_Na} + \left(I_{LCCa\_Na\_iz} + I_{LCCa\_Na\_blk}\right) \quad \text{(Eq. S172)}$$

$$I_{tot\_K} = \left(I_{CaL\_K\_jnc} + I_{CaL\_K\_iz} + I_{CaL\_K\_blk}\right) + I_{NaT\_K} + I_{NaL\_K} + I_{K1\_K} + I_{Kr\_K} + \left(I_{Ks\_K\_iz} + I_{Ks\_K\_blk}\right) + I_{Kto\_K} + I_{Kpl} + I_{NaK\_K} + I_{KATP\_K\_cyt} + I_{bNSC\_K} + \left(I_{LCCa\_K\_iz} + I_{LCCa\_K\_blk}\right) \quad \text{(Eq. S173)}$$

Ion concentrations

$$\frac{d\left[Ca^{2+}{}_{total}\right]_{jnc}}{dt} = -\frac{I_{tot\_Ca\_jnc} \cdot C_m}{V_{jnc} \cdot 2 \cdot F} + \frac{J_{Ca\_rel}}{V_{jnc}} - \frac{J_{Ca\_jnciz}}{V_{jnc}} \quad \text{(Eq. S174)}$$

$$\frac{d\left[Ca^{2+}{}_{total}\right]_{iz}}{dt} = -\frac{I_{tot\_Ca\_iz} \cdot C_m}{V_{iz} \cdot 2 \cdot F} + \frac{J_{Ca\_jnciz}}{V_{iz}} - \frac{J_{Ca\_izblk}}{V_{iz}} \quad \text{(Eq. S175)}$$

$$\frac{d\left[Ca^{2+}{}_{total}\right]_{blk}}{dt} = -\frac{I_{tot\_Ca\_blk} \cdot C_m}{V_{blk} \cdot 2 \cdot F} - \frac{J_{Ca\_SERCA}}{V_{blk}} + \frac{J_{Ca\_izblk}}{V_{blk}} \quad \text{(Eq. S176)}$$

$$\frac{d\left[Ca^{2+}\right]_{SRup}}{dt} = \frac{J_{SERCA}}{V_{SRup}} - \frac{J_{trans\_SR}}{V_{SRup}} \quad \text{(Eq. S177)}$$

$$\frac{d\left[Ca^{2+}{}_{total}\right]_{SRrl}}{dt} = \frac{J_{trans\_SR}}{V_{SRrl}} - \frac{J_{rel\_SR}}{V_{SRrl}} \quad \text{(Eq. S178)}$$

$$\frac{d\left[Na^{+}\right]_i}{dt} = -\frac{I_{tot\_Na} \cdot C_m}{V_{cyt} \cdot F} \quad \text{(Eq. S179)}$$

$$\frac{d\left[K^{+}\right]_i}{dt} = -\frac{\left(I_{tot\_K} + I_{app}\right) \cdot C_m}{V_{cyt} \cdot F} \quad \text{(Eq. S180)}$$

Contraction

The original model of Negroni and Lascano (38) was used. The magnitude of Fb is given in a unit of mN mm^{-2}. The binding of Ca^{2+} to a troponin system (TS) having 3 Ca^{2+} binding sites (given in µM) was included in the equation of determining the concentration of free Ca^{2+} in the bulk compartment.

$$[Ca^{2+}]_{blk} = [Ca_{total}]_{blk} - (CaMCa + TnChCa + SRCa + \frac{3 \cdot (TSCa_3 + TSCa_3^{\sim} + TSCa_3^{*})}{1000}) \quad \text{(Eq. S181)}$$

Supplemental Figures and Tables

Determination of the deactivation rate of a couplon

Determination of the closing rate (Eq. S149) of the Hinch-type couplon model

The closing rate of a couplon may be different from that of single RyR. We addressed this question by comparing the closing rate between a single RyR and a regenerative couplon by examining the statistical distribution of open times, which is described by a monoexponential decay function of the form:

$$f(t) = N_e \cdot e^{-\frac{t}{\tau}} \qquad \text{(Eq. S182)}$$

where *f(t)* is the number of observed open events of life time *t*, N_e is the total number of open events, and τ is the inverse of the transition rate. The two-state transition schemes defined for both RyR and couplon in the present study are,

$C \underset{koc}{\overset{kco}{\rightleftarrows}} O$ for a single RyR, and $C \underset{\beta}{\overset{\alpha}{\rightleftarrows}} O$ for a couplon.

In the following analysis, 10 RyRs (N_{RyR} = 10), which have no co-operativity, were assumed in a single couplon. For simplicity, the couplon closed state was defined as the state when all RyRs were closed, and the open state when one or more RyRs were open at any given time.

The effects of the multiple openings of RyRs within a couplon on the closing rate

Using the transition rates, k_{close} and k_{open}, in the LC model, we calculated the stochastic state transitions of individual RyRs within the couplon and Fig. S3A shows a sample segment of reconstructed time course of state transitions of RyRs. The couplon close times (t_c) are indicated by the thick black bars under the record, and thus the open time (t_o) is indicated by the interval between two sequential black bars. The distribution of t_o was analysed by constructing histograms of number of observation in panel B. An attempt to fit a single exponential using single RyR kinetics (k_{oc}) (Eq. S183) to the histogram (red curve in panel B) was clearly unsatisfactory. The distribution of $f(t_o)$ of a couplon showed a marked deviation from a single exponential at longer t_o events.

$$f(t_o) = N_e \cdot e^{-k_{oc} \cdot t_o} \qquad \text{(Eq. S183)}$$

We assumed that this deviation resulted from multiple open events (MOEs) overlapping with single level opening, which are shown by green bars ($t_{m,i}$) in Fig. S3A. To test this view, we subtracted the sum of $t_{m,i}$ from t_o (Eq. S184) to define a corrected open time (t_o') as in Eq. S184.

$$t_o' = t_o - \sum_{i=1}^{k} t_{m,i} \qquad \text{(Eq. S184)}$$

The red line in Fig. S3B fitted well to the $f(t_o')$ (Eq. S185) in Fig. S3C, suggesting that MOEs are indeed responsible for the deviation of the couplon open dwell time histograms in Fig. S3B from a monoexponential function calculated using single RyR kinetics (k_{oc}) (Eq. S183).

$$f(t_o') = N_e \cdot e^{-k_{oc} \cdot t_o'} \qquad \text{(Eq. S185)}$$

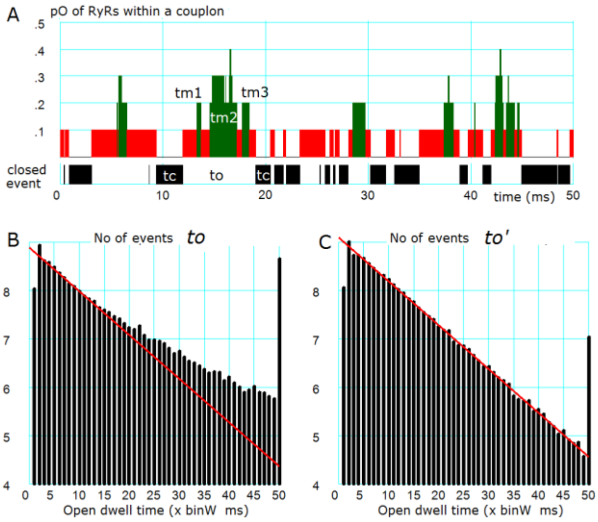

Fig. S3 Dwell time histograms for t_o and t_o' obtained from stochastic calculation of a couplon consisting of RyRs (N_{RyR} = 10) at $[Ca]_{nd}$ = 50μM. A: probability of open RyRs within a couplon. Black, red and green colours indicate durations that none, one, or multiple RyRs are open at the time. The closed, open, and multiple open time durations are indicated by t_c, t_o and t_{mi} (i = 1~k), respectively. B; dwell time histogram for t_o, fitted with a monoexponential function with $\tau = 1/k_{oc}$. C: dwell time histogram for t_o', fitted with the same monoexponential function as in B. The large number of events at the last bin in the histogram are the sum of events observed at longer open dwell time than the maximum value of 50 × 0.1 (binwidth) = 5 ms.

Determination of closing rate of a couplon, β

According to the findings described above, the closing rate of a couplon (β) might be determined from the closing rate k_{oc} of RyR, provided that the fraction t_o'/t_o is predicted. Based on the fact that all the remaining RyRs (N_{RyR} - 1) are closed during t_o' except the single open RyR, this probability of simultaneous closure of (N_{RyR} - 1) RyRs will be approximated by $pC^{(N_{RyR}-1)\cdot l}$.

$$t_o' \approx g(t_o) = t_o \cdot pC^{(N_{RyR}-1)\cdot l} \quad or \quad \frac{t_o'}{t_o} \approx pC^{(N_{RyR}-1)\cdot l} \qquad \text{(Eq. S186)}$$

where pC is the steady state closed probability of a single RyR (Eq. S187), and l is a correction factor.

$$pC = \frac{k_{oc}}{k_{co} + k_{oc}} \qquad \text{(Eq. S187)}$$

Then, the distribution of couplon open times t_o is given by,

$$f(g(t_o)) \approx N_e \cdot e^{-k_{oc}\cdot t_o \cdot pC^{(N_{RyR}-1)\cdot l}} = N_e \cdot e^{-\beta \cdot t_o} \qquad \text{(Eq. S188)}$$

and

$$\beta = k_{oc} \cdot pC^{(N_{RyR}-1)\cdot l}. \qquad \text{(Eq. S189)}$$

Lastly, we fixed the correction factor, l, by performing stochastic simulations for various $[Ca]_{nd}$. We calculated the ensemble average of N_e = 5000 open events as shown by an example at 50 μM $[Ca]_{nd}$ in Fig. S4A, which was well fitted with a single exponential function (red curve) using the least squares method. The closing rates of a couplon thus obtained at various $[Ca]_{nd}$ are plotted in Fig. S4B for the LC model (red). The same analysis was also applied to our couplon model in HuVEC model and results were plotted by black symbols. The two continuous curves, red and black superimposed on the data points, were drawn by Eq. S189 using a common l fixed at 0.74. We also confirmed that Eq. S189 was applicable to couplons consisting of 1~20 RyRs.

In brief, we conclude that the closing rate defined by the two state transition model of a couplon is different from that of single RyR kinetics because of overlaps of MOEs during the 'open time of a couplon'.

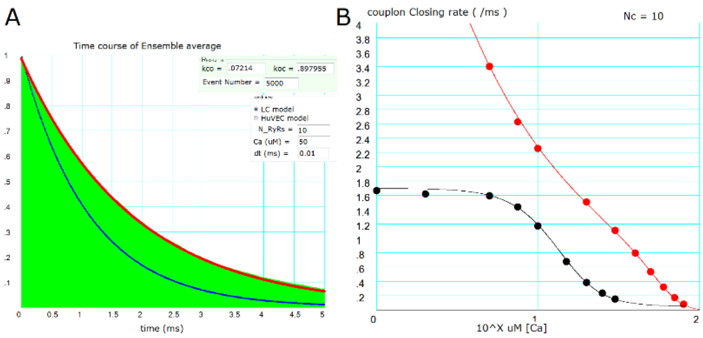

Fig. S4 Determination of the closing rate β for the two-state couplon model.

A: Ensemble mean of couplon open times. The ensemble mean of open times (t_o) was constructed by cumulating individual open events during the course of stochastic computation of 10 RyRs within a couplon until 5000 events were accumulated (Green area) by applying 50 μM $[Ca]_{nd}$ to the LC model. The red exponential curve was fitted by the least squares method. The blue exponential curve was drawn using the k_{oc} of single RyR for comparison. B: Red circles illustrate data points of β obtained by applying the least squares method to the ensemble mean at various $[Ca]_{nd}$ indicated on the abscissa of logarithmic scale. The continuous curve was drawn by the empirical formula of Eq. S189 with l = 0.74. Red symbols are derived from the couplon of LC model, and black symbols are from that of HuVEC model.

Comparison of activation and deactivation rates of a RyR or couplon among different models

In the SJ, LC, SM(toy) and our HuVEC models, the gating of a single RyR is described using the two-state kinetic scheme, and the rate constants are based on the single channel recordings in the planar lipid bilayer method. The activation rates are all dependent on $[Ca^{2+}]$ with a cooperativity factor (n_H) of 2 ~ 4. In our model, the activation rate of a single RyR (red line) was determined by adjusting the rate used in SM model (blue line).

Table S6 Comparisons among mathematical descriptions of the couplon activation

	Spark CICR model		Whole cell CICR model	
	SJ model	SM 'toy' model	HuVEC model	Hinch model
Activation rate	$\dfrac{k_o \cdot CF_{open}}{1+(\frac{K}{Ca})^4}$	$k_o \cdot Ca^2 \cdot (sloc0+Ca_{sr})$ $Ca = \dfrac{i \cdot n_{open}}{8\pi FhD} + cao$	$\overline{k_{rco}}$ (Eq. 9) $k_{rco} = (f_n \cdot k_{co}) \cdot f_t \cdot (sloc0 + Ca_{SRrl})$ $k_{co}(Ca_{LR/0R}) = \dfrac{1}{1+(\frac{K}{Ca_{nd}})^{2.7}}$ $f_t = \dfrac{k_{co}(Ca_{L0/00})}{k_{co}(Ca_{L0/00}) + k_c}$	$\dfrac{k_o}{1+(\frac{K}{Ca_{L0/00}})^2}$
Deactivation rate	$k_c \cdot CF_{close}$	kc	$k_c \cdot pC^{(N_{RyR}-1)\cdot l}$	kc
Reference local Ca^{2+} for RyR or couplon activation	$\dfrac{d[Ca]_{ss}}{dt} = J_{LCC} + J_{RyR} + J_D$	$[Ca]_{dc} = f_{SMtoy}(J_{RyR})$	$[Ca]_{nd} = f_{HuVEC}(J_{LCC}, J_{RyR}, [Ca]_{jnc}, [Ca]_{SRrl}, [Ca]_o)$ (Eq. 2)	$[Ca]_{ds} = f_{Hinch}(J_{LCC}, [Ca]_i)$
next compartment	*blk*	*n.c*	*jnc*	*blk*

k_o, k_c; opening and closing rate constants of a RyR, CF_{open} and CF_{close}; cooperative factor for open and close rate, *i*; single RyR channel current, (sloc0+Ca_{sr}); the SR Ca^{2+}-content factor, *pC*; probability of closed state, N_{RyR}; number of RyRs within a couplon, *l*; correcting factor, *ss*; subspace, *dc*; dyadic cleft, ds; dyadic space, K; a half saturation [Ca^{2+}], J_X; Ca^{2+} flux via X per unit volume and n.c.; not concerned. No empirical equations are given in LC model.

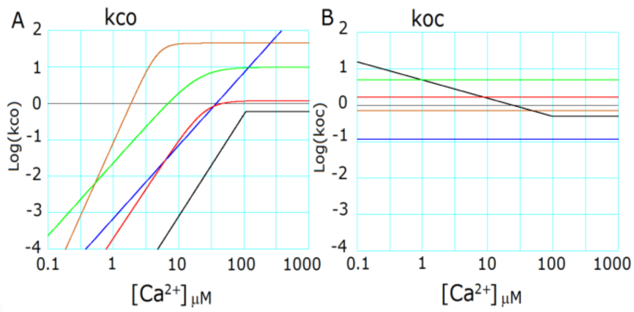

Fig. S5. Kinetics of RyRs

Relationships between [Ca^{2+}] and open (Fig. S5A) and close rates (Fig. S5B), in five model studies are shown in each panel respectively. Black: LC model, Blue: SM model, Lime: Hinch model, Chocolate: SJ model, Red: HuVEC model. A [Ca^{2+}]$_{SRrl}$ of 500 μM was used to calculate rate of activation if necessary.

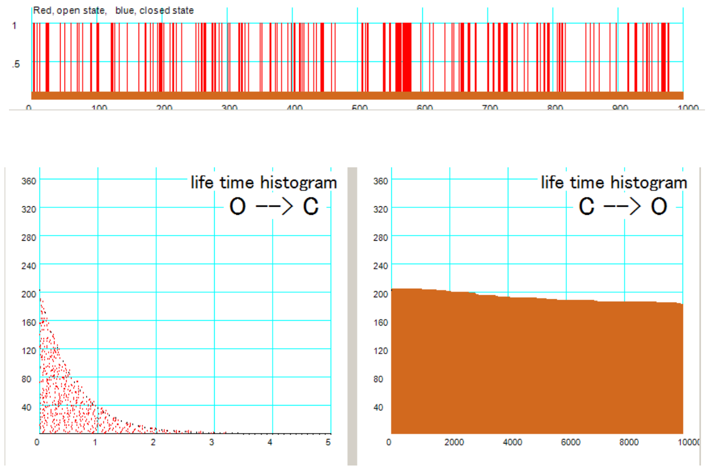

Fig. S6. Stochastic simulation of 20,000 couplons activity and its life time histogram (Ca00=0.2uM, SRCa=0.6mM, Ca0R=0.15mM). Top) red vertical lines show 203 open events of 20,000 couplons occurred in 1000 ms. Bottom: open and close life time histogram obtained after 20,000 sweeps of stochastic simulations including 196 open events show smoothed time courses of the activation and inactivation of couplons.

Implementation of 'blink space (*bs*)' in HuVEC model

In order to examine the involvement of 'blinks' in determining the time course of CICR extinction, we newly assume a 'blink space' (*bs*) under the junctional SR membrane supporting the couplon as schematically shown in Fig. S7. The parameters in this figure are denoted in analogy to the HuVEC (Hinch) dyadic space model.

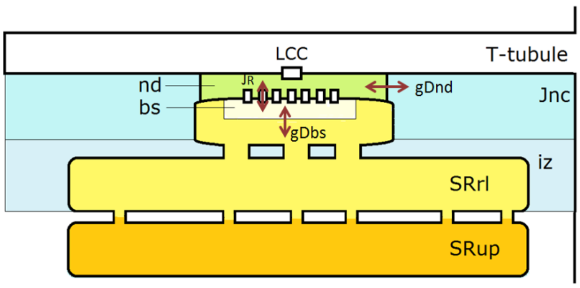

Fig. S7. Schematic representation of the dyadic model. J_R; Ca^{2+} permeability of single couplon (μm^3/ms), gD_{bs}; Ca^{2+} flux rate from *SRrl* to *bs* (μm^3/ms), gD_{nd}; Ca^{2+} flux rate from *nd* to *jnc* (μm^3/ms), Ca_{bs}; Ca^{2+} concentration in *bs* (mM), Ca_{SRrl}; Ca^{2+} concentration in *SRrl* (mM).

According to the simultaneous recording of both sparks and blinks (39-41) the time course of a blink is nearly a mirror image of a spark, indicating that the depletion and the replenishment of Ca^{2+} in *bs* is quite rapid. Since each pair of spark-blink of a similar time course is evoked by the same Ca^{2+} flux via a couplon, the balance between the Vol_{bs} and gD_{bs} should be comparable to that between Vol_{nd} and gD_{nd}. If so, $[Ca^{2+}]_{bs}$ (Ca_{bs}) might be given as an instantaneous function of J_R and gD_{bs} in analogy to $[Ca^{2+}]_{ds}$ in the Hinch formalism. The rate of change in Ca_{bs} is,

$$\frac{dCa_{bs}}{dt} = \frac{-J_R \cdot (Ca_{bs} - Ca_{nd}) + gD_{bs} \cdot (Ca_{SRrl} - Ca_{bs})}{Vol_{bs}} \quad \text{(Eq. S190)}$$

If a rapid equilibrium of Ca^{2+} diffusion is assumed within the blink space in Eq. S190, namely, $dCa_{bs}/dt = 0$

$$J_R \cdot (Ca_{bs} - Ca_{nd}) = gD_{bs} \cdot (Ca_{SRrl} - Ca_{bs}) \ . \quad \text{(Eq. S191)}$$

Eq. S191 is comparable to the original Hinch algorithm for the instantaneous balance of Ca^{2+} fluxes at *nd*.

$$J_R \cdot (Ca_{bs} - Ca_{nd}) = gD_{nd} \cdot (Ca_{nd} - Ca_{00}) \quad \text{(Eq. S192)}$$

From Eqs. S191 & S192, Ca_{bs} and Ca_{nd} is given as an instantaneous function of Ca_{00} and Ca_{SRrl}. For example, when a couplon is open and LCC is closed, Ca_{bs} and Ca_{nd} are determined by Eqs. S193 & S194.

$$Ca_{bs} = \frac{\dfrac{Ca_{00}}{1+f_R} + \dfrac{Ca_{SRrl}}{f_{bs}}}{(1 + \dfrac{1}{f_{bs}} - \dfrac{f_R}{1+f_R})} \quad \text{(Eq. S193)}$$

and

$$Ca_{nd} = Ca_{0R} = \frac{Ca_{00} + f_R \cdot Ca_{bs}}{1+f_R}, \quad \text{(Eq. S194)}$$

where

$$f_R = \frac{J_R}{gD_{nd}} \quad \text{(Eq. S195)}$$

and

$$f_{bs} = \frac{J_R}{gD_{bs}} \ . \quad \text{(Eq. S196)}$$

When the couplon is closed,

$$Ca_{bs} = Ca_{SRrl} \ . \quad \text{(Eq. S197)}$$

Namely, Ca_{bs} switches between these two concentrations according to the open-close transitions of the couplon. This instantaneous relationship of Ca_{bs} can be readily applied to the compound state transition model of CaRU (36). When $gD_{bs} = \infty$, then $Ca_{bs} = Ca_{SRrl}$ and $Ca_{nd} = Ca_{0R}$ as in the original HuVEC model, and when $gD_{bs} = 0$, then $Ca_{bs} = Ca_{nd} = Ca_{00}$.

Using the dyadic model newly developed as above, the relationship between the degree of local SR depletion and the activation and deactivation of a couplon, (k_{rco} and k_{roc}), was determined by varying the ratio of gD_{bs} and gD_{nd} ($r_{bs} = gD_{bs} / gD_{nd}$) at various levels of Ca_{SRrl} (Fig. S8).

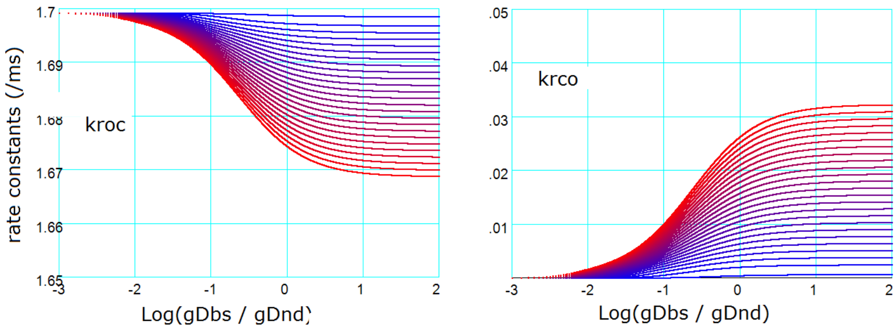

Fig. S8. Rate constants calculated using the dyadic model at various r_{bs} (Ca00=2 μM, $[Ca^{2+}]_{SRrl}$=0.1~5 mM). $[Ca^{2+}]_{SRrl}$ was changed to various levels from 0.1 to 5 mM in increments of 0.2 mM. k_{roc} and k_{rco} was colored in a gradient manner according to $[Ca^{2+}]_{SRrl}$ (blue at $[Ca^{2+}]_{SRrl}$ = 0.1mM and red at $[Ca^{2+}]_{SRrl}$ = 5 mM).

Considering $[Ca^{2+}]_{SRrl}$ = ~0.6 mM at resting condition, it may be concluded that a single couplon could exhibit a train of open events at higher $[Ca^{2+}]_{SRrl}$, which would be achieved by increasing Ca^{2+} flux rate from SRrl to *bs* (gD_{bs}) or SR Ca^{2+} loading by, for example, pharmacological treatment.

Frequency-dependency of HuVEC model

For validation of HuVEC model, the frequency-dependencies of $[Na^+]_{cyt}$, APD_{90}, $[Ca^{2+}]_{SRrl}$ and the peak amplitude of Ca^{2+} transient were examined (Fig. S9). At every stimulus frequency, all these measurements reached stable values, and responses were completely reversible after returning to the control frequency. The APD_{90} smoothly decreased with increasing stimulation rate as reported in both experimental and simulation studies (21, 24, 42-44). This decrease of APD_{90} was largely due to the increase in outward I_{NaK} amplitude induced by the accumulation of $[Na^+]_{cyt}$ with increasing frequency of AP generation. The decrease in $[Ca^{2+}]_{SRrl}$ at the lower stimulus frequency was due to the Ca^{2+} leak from SR via basal openings of RyRs during diastole, while the decrease with increasing frequency above 1 Hz was due to incomplete replenishment of SR with Ca^{2+} during the shortened diastolic duration. Nevertheless, the peak of $[Ca^{2+}]_{blk}$ transient was increased with increasing frequency. This is because the diastolic level of $[Ca^{2+}]_{blk}$ was elevated, for example from the control 0.064 μM to 0.16 μM at 2.5 Hz. The shortening of APD was well correlated with the increase in $I_{Na/K}$ with increasing $[Na^+]_{cyt}$. These findings are in line with the GPB and ORd models.

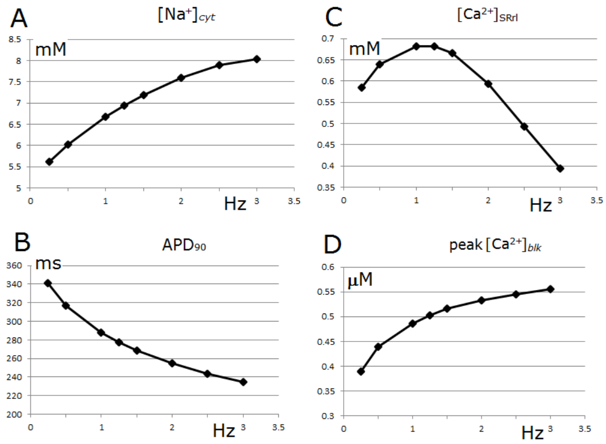

Fig. S9. Frequency-dependency of the HuVEC model

A: $[Na^+]_{cyt}$, B: APD_{90}, C: $[Ca^{2+}]_{SRrl}$, D: peak $[Ca^{2+}]_{blk}$ magnitude of isotonic F_b at 6 mN/mm^2. The ion concentrations were measured at the end of diastole.

Initial set of time-dependent variables of HuVEC model at a standard CL of 1000 ms

Vm = -91.4466885079348
TnChCa = 0.110742559707052
CaMCa = 0.000228581865602447
bufferSRCa = 0.00172960014640511
Lb_jnc = 0.0218215322629436
Lb_iz = 0.0075621764602356
Hb_jnc = 0.185094540066232
Hb_iz = 0.0769149150028914

Nai = 6.66894310282034
Ki = 139.238265011042
Catot_jnc = 0.207176351449979
Catot_iz = 0.084640522722006
Catot_blk = 0.11279654524634
Ca_SRup = 0.761077662687456
Catot_SRrl = 2.21876221622152

O_TM = 0.000000706725155695262
I2_TM = 0.0117704053067285
Is_TM = 0.304002781414015

O_LSM = 0.00000295214591324261
I1_LSM = 0.00254273877063925
I2_LSM = 0.0118261382165599
Is_LSM = 0.303220346353844

Yco_iz = 0.992251726297519
Yoc_iz = 0.00000024556270151713
Yoo_iz = 0.00000314564543512061
Yco_blk = 0.992424981547859
Yoc_blk = 0.000000240070147854924
Yoo_blk = 0.00000314619469048683

Yooo = 0.00000172489315884865
Yooc = 0.00000142034754677507

Ycoo = 0.0000138422676498755
Ycoc = 0.992110534408681
Ycco = 0.0000000953816272498217
Yoco = 0.000000000000156949238162028
Yocc = 0.0000000249594301562175

paraxrF = 0.00000486210633393005
paraxrS = 0.437041249050081

paraxs1_iz = 0.277482694590328
paraxs2_iz = 0.000131110342877451
paraxs1_blk = 0.277482694590328
paraxs2_blk = 0.000131110342877451

a_IKto = 0.000793627635934239
y1_IKto = 0.999756080468878
y2_IKto = 0.575995954010486

Pbspm = 0.594875991179992

E1NCX_iz = 0.238718640001014
I1NCX_iz = 0.13771129457898
I2NCX_iz = 0.622892868847556
E1NCX_blk = 0.111872123711613
I1NCX_blk = 0.203023555446362
I2NCX_blk = 0.684869019924837

P1_6_NaK = 0.435289193632868
P7_NaK = 0.0831770174499825
P8_13_NaK = 0.281082409575779

halfSL = 1.09840500012898
Fb = 0.0502092089156129
Fp = 4.94926096641491
TSCa3 = 0.00899891910620064
TSCa3W = 0.000369547640656701
TSCa3S = 0.000153834503967436
TSS = 0.000876347322180234
TSW = 0.000492054058977473
hw = 0.000100147615113241
hp = 0.00600014761511324

ATPt_cyt = 6.67701543987464
ADPt_cyt = 0.0227671477707
Pi_cyt = 0.381130087573153
PCr_cyt = 13.9261301893242

Supporting References

1. Beuckelmann, D. J., M. Nabauer, and E. Erdmann. 1992. Intracellular calcium handling in isolated ventricular myocytes from patients with terminal heart failure. Circulation 85:1046-1055.
2. Powell, T., M. F. Sturridge, S. K. Suvarna, D. A. Terrar, and V. W. Twist. 1981. Intact individual heart cells isolated from human ventricular tissue. British medical journal 283:1013-1015.
3. Satoh, H., L. M. Delbridge, L. A. Blatter, and D. M. Bers. 1996. Surface:volume relationship in cardiac myocytes studied with confocal microscopy and membrane capacitance measurements: species-dependence and developmental effects. Biophysical journal 70:1494-1504.
4. Jost, N., L. Virag, M. Bitay, J. Takacs, C. Lengyel, P. Biliczki, Z. Nagy, G. Bogats, D. A. Lathrop, J. G. Papp, and A. Varro. 2005. Restricting excessive cardiac action potential and QT prolongation: a vital role for IKs in human ventricular muscle. Circulation 112:1392-1399.
5. Sakakibara, Y., T. Furukawa, D. H. Singer, H. Jia, C. L. Backer, C. E. Arentzen, and J. A. Wasserstrom. 1993. Sodium current in isolated human ventricular myocytes. The American journal of physiology 265:H1301-1309.
6. Mewes, T., and U. Ravens. 1994. L-type calcium currents of human myocytes from ventricle of non-failing and failing hearts and from atrium. Journal of molecular and cellular cardiology 26:1307-1320.
7. Li, G. R., J. Feng, L. Yue, M. Carrier, and S. Nattel. 1996. Evidence for two components of delayed rectifier K+ current in human ventricular myocytes. Circulation research 78:689-696.
8. Iost, N., L. Virag, M. Opincariu, J. Szecsi, A. Varro, and J. G. Papp. 1998. Delayed rectifier potassium current in undiseased human ventricular myocytes. Cardiovascular research 40:508-515.
9. Gerdes, A. M., S. E. Kellerman, J. A. Moore, K. E. Muffly, L. C. Clark, P. Y. Reaves, K. B. Malec, P. P. McKeown, and D. D. Schocken. 1992. Structural remodeling of cardiac myocytes in patients with ischemic cardiomyopathy. Circulation 86:426-430.
10. Laver, D. R., C. H. Kong, M. S. Imtiaz, and M. B. Cannell. 2013. Termination of calcium-induced calcium release by induction decay: an emergent property of stochastic channel gating and molecular scale architecture. Journal of molecular and cellular cardiology 54:98-100.
11. Sobie, E. A., K. W. Dilly, J. dos Santos Cruz, W. J. Lederer, and M. S. Jafri. 2002. Termination of

cardiac Ca(2+) sparks: an investigative mathematical model of calcium-induced calcium release. Biophysical journal 83:59-78.

12. Shannon, T. R., F. Wang, J. Puglisi, C. Weber, and D. M. Bers. 2004. A mathematical treatment of integrated Ca dynamics within the ventricular myocyte. Biophysical journal 87:3351-3371.

13. Asakura, K., C. Cha, H. Yamaoka, Y. Horikawa, H. Memida, T. Powell, A. Amano, and A. Noma. 2014. EAD and DAD mechanisms analyzed by developing a new human ventricular cell model. Progress in biophysics and molecular biology.

14. Negroni, J. A., and E. C. Lascano. 2008. Simulation of steady state and transient cardiac muscle response experiments with a Huxley-based contraction model. Journal of molecular and cellular cardiology 45:300-312.

15. Yue, D. T., and E. Marban. 1990. Permeation in the dihydropyridine-sensitive calcium channel. Multi-ion occupancy but no anomalous mole-fraction effect between Ba^{2+} and Ca^{2+}. The Journal of general physiology 95:911-939.

16. Peterson, B. Z., J. S. Lee, J. G. Mulle, Y. Wang, M. de Leon, and D. T. Yue. 2000. Critical determinants of Ca(2+)-dependent inactivation within an EF-hand motif of L-type Ca(2+) channels. Biophysical journal 78:1906-1920.

17. Shirokov, R., R. Levis, N. Shirokova, and E. Rios. 1993. Ca(2+)-dependent inactivation of cardiac L-type Ca2+ channels does not affect their voltage sensor. The Journal of general physiology 102:1005-1030.

18. Ferreira, G., J. Yi, E. Rios, and R. Shirokov. 1997. Ion-dependent inactivation of barium current through L-type calcium channels. The Journal of general physiology 109:449-461.

19. Pelzmann, B., P. Schaffer, E. Bernhart, P. Lang, H. Machler, B. Rigler, and B. Koidl. 1998. L-type calcium current in human ventricular myocytes at a physiological temperature from children with tetralogy of Fallot. Cardiovascular research 38:424-432.

20. Magyar, J., N. Iost, A. Kortvely, T. Banyasz, L. Virag, P. Szigligeti, A. Varro, M. Opincariu, J. Szecsi, J. G. Papp, and P. P. Nanasi. 2000. Effects of endothelin-1 on calcium and potassium currents in undiseased human ventricular myocytes. Pflugers Archiv : European journal of physiology 441:144-149.

21. Li, G. R., J. Feng, L. Yue, and M. Carrier. 1998. Transmural heterogeneity of action potentials and Ito1 in myocytes isolated from the human right ventricle. The American journal of physiology 275:H369-377.

22. Fulop, L., T. Banyasz, J. Magyar, N. Szentandrassy, A. Varro, and P. P. Nanasi. 2004. Reopening of L-type calcium channels in human ventricular myocytes during applied epicardial action potentials. Acta physiologica Scandinavica 180:39-47.

23. Brunet, S., T. Scheuer, and W. A. Catterall. 2009. Cooperative regulation of Ca(v)1.2 channels by intracellular Mg(2+), the proximal C-terminal EF-hand, and the distal C-terminal domain. The

Journal of general physiology 134:81-94.

24. Grandi, E., F. S. Pasqualini, and D. M. Bers. 2010. A novel computational model of the human ventricular action potential and Ca transient. Journal of molecular and cellular cardiology 48:112-121.

25. Sun, L., J. S. Fan, J. W. Clark, and P. T. Palade. 2000. A model of the L-type Ca^{2+} channel in rat ventricular myocytes: ion selectivity and inactivation mechanisms. The Journal of physiology 529 Pt 1:139-158.

26. Zhang, J. F., P. T. Ellinor, R. W. Aldrich, and R. W. Tsien. 1994. Molecular determinants of voltage-dependent inactivation in calcium channels. Nature 372:97-100.

27. Matsuda, H. 1986. Sodium conductance in calcium channels of guinea-pig ventricular cells induced by removal of external calcium ions. Pflugers Archiv : European journal of physiology 407:465-475.

28. Yan, D. H., and K. Ishihara. 2005. Two Kir2.1 channel populations with different sensitivities to Mg(2+) and polyamine block: a model for the cardiac strong inward rectifier K(+) channel. The Journal of physiology 563:725-744.

29. Ishihara, K., and D. H. Yan. 2007. Low-affinity spermine block mediating outward currents through Kir2.1 and Kir2.2 inward rectifier potassium channels. The Journal of physiology 583:891-908.

30. Jost, N., L. Virag, P. Comtois, B. Ordog, V. Szuts, G. Seprenyi, M. Bitay, Z. Kohajda, I. Koncz, N. Nagy, T. Szel, J. Magyar, M. Kovacs, L. G. Puskas, C. Lengyel, E. Wettwer, U. Ravens, P. P. Nanasi, J. G. Papp, A. Varro, and S. Nattel. 2013. Ionic mechanisms limiting cardiac repolarization reserve in humans compared to dogs. The Journal of physiology 591:4189-4206.

31. Rajamani, S., L. L. Eckhardt, C. R. Valdivia, C. A. Klemens, B. M. Gillman, C. L. Anderson, K. M. Holzem, B. P. Delisle, B. D. Anson, J. C. Makielski, and C. T. January. 2006. Drug-induced long QT syndrome: hERG K^+ channel block and disruption of protein trafficking by fluoxetine and norfluoxetine. British journal of pharmacology 149:481-489.

32. Takeuchi, A., S. Tatsumi, N. Sarai, K. Terashima, S. Matsuoka, and A. Noma. 2006. Ionic mechanisms of cardiac cell swelling induced by blocking Na^+/K^+ pump as revealed by experiments and simulation. The Journal of general physiology 128:495-507.

33. Oka, C., C. Y. Cha, and A. Noma. 2010. Characterization of the cardiac Na^+/K^+ pump by development of a comprehensive and mechanistic model. Journal of theoretical biology 265:68-77.

34. Smith, N. P., and E. J. Crampin. 2004. Development of models of active ion transport for whole-cell modelling: cardiac sodium-potassium pump as a case study. Progress in biophysics and molecular biology 85:387-405.

35. Grandi, E., F. S. Pasqualini, C. Pes, C. Corsi, A. Zaza, and S. Severi. 2009. Theoretical

investigation of action potential duration dependence on extracellular Ca^{2+} in human cardiomyocytes. Journal of molecular and cellular cardiology 46:332-342.

36. Hinch, R., J. L. Greenstein, A. J. Tanskanen, L. Xu, and R. L. Winslow. 2004. A simplified local control model of calcium-induced calcium release in cardiac ventricular myocytes. Biophysical journal 87:3723-3736.

37. Tran, K., N. P. Smith, D. S. Loiselle, and E. J. Crampin. 2009. A thermodynamic model of the cardiac sarcoplasmic/endoplasmic Ca(2+) (SERCA) pump. Biophysical journal 96:2029-2042.

38. Negroni, J. A., and E. C. Lascano. 1996. A cardiac muscle model relating sarcomere dynamics to calcium kinetics. Journal of molecular and cellular cardiology 28:915-929.

39. Brochet, D. X., D. Yang, A. Di Maio, W. J. Lederer, C. Franzini-Armstrong, and H. Cheng. 2005. Ca^{2+} blinks: rapid nanoscopic store calcium signaling. Proceedings of the National Academy of Sciences of the United States of America 102:3099-3104.

40. Zima, A. V., E. Picht, D. M. Bers, and L. A. Blatter. 2008. Termination of cardiac Ca^{2+} sparks: role of intra-SR [Ca^{2+}], release flux, and intra-SR Ca^{2+} diffusion. Circulation research 103:e105-115.

41. Brochet, D. X., W. Xie, D. Yang, H. Cheng, and W. J. Lederer. 2011. Quarky calcium release in the heart. Circulation research 108:210-218.

42. Li, G. R., B. Yang, J. Feng, R. F. Bosch, M. Carrier, and S. Nattel. 1999. Transmembrane ICa contributes to rate-dependent changes of action potentials in human ventricular myocytes. The American journal of physiology 276:H98-H106.

43. Pieske, B., B. Kretschmann, M. Meyer, C. Holubarsch, J. Weirich, H. Posival, K. Minami, H. Just, and G. Hasenfuss. 1995. Alterations in intracellular calcium handling associated with the inverse force-frequency relation in human dilated cardiomyopathy. Circulation 92:1169-1178.

44. O'Hara, T., L. Virag, A. Varro, and Y. Rudy. 2011. Simulation of the undiseased human cardiac ventricular action potential: model formulation and experimental validation. PLoS computational biology 7:e1002061.